Available online at www.sciencedirect.com
ScienceDirect
Regulatory Peptides 145 (2008) 7–11
REGULATORY PEPTIDES
www.elsevier.com/locate/regpep

Review

Ghrelin deficiency does not influence feeding performance

Takahiro Sato [a,*], Mamoru Kurokawa [b], Yoshiki Nakashima [a], Takanori Ida [a], Tomoko Takahashi [a], Yoshihiko Fukue [a], Masahito Ikawa [d], Masaru Okabe [d], Kenji Kangawa [c], Masayasu Kojima [a,*]

[a] *Molecular genetics, Institute of Life Sciences, Kurume University, B-3, Kurume research center building, 1-1, Hyakunen-koen, Kurume, 839-0864, Japan*
[b] *Department of Anatomy, Nagasaki University School of Medicine, Nagasaki 852-8523, Japan*
[c] *Department of Biochemistry, National Cardiovascular Center Research Institute, Suita 565-8565, Japan*
[d] *Department of Experimental Genome Research, Genome Information Research Center, Osaka University, Suita 565-0871, Japan*

Available online 18 September 2007

Abstract

Ghrelin is an endogenous ligand for the growth hormone secretagogue receptor that is synthesized predominantly in the stomach. Previous studies demonstrated that ghrelin stimulates growth hormone release and food intake. These data suggested that antagonism of ghrelin could serve as a useful treatment for eating disorders and obesity. To study the role of endogenous ghrelin in feeding performance further, we generated ghrelin-deficient ($ghrl^{-/-}$) mice. Unexpectedly, $ghrl^{-/-}$ mice exhibited normal growth, cumulative food intake, reproduction, histological characters, and serum parameters. There were no differences in feeding patterns between $ghrl^{+/+}$ and $ghrl^{-/-}$ mice. $Ghrl^{-/-}$ mice displayed normal responses to scheduled feedings as seen for $ghrl^{+/+}$ mice. Memory-related feeding performances of $ghrl^{-/-}$ mice were indistinguishable from $ghrl^{+/+}$ littermates. These data indicate that ghrelin is not critical for feeding performance.

Keywords: Ghrelin knockout mouse; Feeding pattern; Memory

Contents

* Corresponding authors. Tel.: +81 942 37 6313; fax: +81 942 31 5212.
E-mail address: mkojima@lsi.kurume-u.ac.jp (M. Kojima).

0167-0115/$ - see front matter © 2007 Elsevier B.V. All rights reserved.
doi:10.1016/j.regpep.2007.09.010

1. Introduction

Ghrelin is an endogenous ligand for the growth hormone secretagogue receptor (GHS-R) [1]. Ghrelin is primarily released from the stomach, but is also secreted from the duodenum and pancreas [1,2]. Peripherally-produced ghrelin influences pituitary hormone secretion, appetite, metabolism, gastrointestinal function, cardiovascular performance, and immune responses. Recently, we characterized ghrelin within the rat hypothalamus [3]; the physiological role(s) of ghrelin secreted from the hypothalamus, however, remains unclear.

Histological analysis indicated that ghrelin receptors localize to a variety of brain regions, including the suprachiasmatic nucleus (SCN) and arcuate nucleus (Arc) within the hypothalamus and the hippocampus [4]. The SCN is important region functioning in the regulation of circadian rhythms, while the Arc plays a primary role in feeding control. The hippocampus has a central role in the regulation of memory. Hypothalamic ghrelin also localizes to the Arc [3]; intracerebroventricular injection of ghrelin induces gene expression of neuropeptide Y and agouti-related peptide and impairs the electrical activity of proopiomelanocortin neurons [5–8]. These results indicate that hypothalamic ghrelin regulates feeding patterns and memory related to feeding.

In this study, we sought to investigate if ghrelin regulates feeding performances by generating ghrelin knockout mice.

2. Materials and methods

2.1. Animal care

All animal protocols were approved by the Ethical Committee for the Research of Life Science of Kurume University. All mice were housed in a 7 a.m. to 7 p.m. light cycle. All experiments were performed with F6 littermate pairs; mice were individually caged during experiments.

2.2. Generation of $ghrl^{-/-}$ mice

These animals will be described in detail in another report. All exons were replaced by a neo cassette. Targeted ES cells and resultant wild-type ($ghrl^{+/+}$), heterozygous ($ghrl^{+/-}$), and homozygous ($ghrl^{-/-}$) pups were genotyped by Southern blot analysis using a 5′-probe, 3′-probe, and exon probe.

2.3. Preparation to tissue and ELISA

To confirm the absence of ghrelin from the stomachs of $ghrl^{-/-}$ mice, tissues were quickly removed after mice were sacrificed. Each sample was diced and boiled for 5 min in a 10-fold volume of water to inactive intrinsic proteases. After cooling, solutions were adjusted to final concentrations of 1 M AcOH and 20 mM HCl. Tissues were homogenized with a Polytron mixer; after centrifugation at 15,000 rpm for 10 min, supernatants were loaded onto Sep-Pak C18 cartridges (Waters, Milford, MA). Cartridges were then washed in 0.9% NaCl and 10% CH_3CN/0.1% TFA before bound peptide was eluted with 60% CH_3CN/0.1% TFA. The eluate was lyophilized and analyzed using an active ghrelin ELISA Kit (Mitsubishi Kagaku Iatron, Inc., Tokyo, Japan).

2.4. Immunohistochemistry

Mice was perfused with 4% PFA solution and embedded in paraffin. Immunohistochemical staining of ghrelin was performed using the avidin–biotinylated-enzyme complex (ABC) method in conjunction with a VECTASTAIN ABC-PO kit (Vector Laboratories Inc., Burlingame, CA). Immunostaining was performed as previously described [3,9]. Briefly, sections were deparaffinized in xylene and a graded series of ethanol. Sections were then pretreated with 3% hydrogen peroxide in methanol for 5 min to endogenous peroxidase activity. After rinsing with PBS, sections were treated for 30 min with 1.5% normal goat serum, then incubated with polyclonal rabbit anti-ghrelin antibody (#6-6; diluted 1:80,000) for 16 h at 4 °C. Sections were rinsed in PBS and incubated with biotinylated anti-rabbit IgG for 40 min. After rinsing in PBS, sections were incubated with avidin–biotinylated regents for 1 h. Sections were visualized with DAB solution (DAKO, Kyoto, Japan).

2.5. The analysis of feeding performance and memory

$Ghrl^{-/-}$ mice were housed in a K2-CABIN apparatus (Phenotype analyzing, Nagasaki, Japan) and given a powder diet (CREA, Tokyo, Japan) to estimate feeding patterns. Animals were given free access to feed and water. Using this system, we recorded the amounts of food and water intake every 15 min for 12 days. To reveal the adaptation capability of mice to a negative energy state, we instituted scheduled feedings. Mice were given feeds for a 4 h period only from 9 a.m. to 1 p.m. We then measured the 4-h food intake at 1 p.m. To investigate memory in $ghrl^{-/-}$ mice, mice were housed in the KUROBOX apparatus (Phenotype analyzing, Nagasaki, Japan) [10].

2.6. Statistical analysis

Results are presented as the means±SD for each group. Comparisons between groups were made using ANOVA with a Williams test. $P<0.05$ was accepted as statistically significant.

3. Results

3.1. Target disruption of the ghrl locus

Loss of the *ghrl* allele was confirmed by southern blot and PCR analysis of DNA isolated from $ghrl^{+/+}$, $ghrl^{+/-}$, and $ghrl^{-/-}$ mice (data not shown). Measurement of ghrelin levels by ELISA indicated that the stomachs of $ghrl^{-/-}$ mice did not contain ghrelin. Immunohistochemistry also demonstrated the absence of ghrelin-producing cells in the stomachs of $ghrl^{-/-}$ mice (data not shown). We observed a normal birth ratio of $ghrl^{+/+}$, $ghrl^{+/-}$, and $ghrl^{-/-}$ mice as predicted by Mendelian genetics ($ghrl^{+/+}$: $ghrl^{+/-}$: $ghrl^{-/-}$=243 : 498 : 257). All

ghrl$^{-/-}$ mice appeared grossly normal, undergoing normal development to reach adulthood. Male *ghrl*$^{+/+}$, *ghrl*$^{+/-}$, and *ghrl*$^{-/-}$ mice had similar body weights at all ages (Fig. 1A).

3.2. Feeding pattern of *ghrl*$^{-/-}$ mice

We hypothesized that ghrelin plays a major role in promoting appetite and regulating feeding patterns. To test this hypothesis, we tested if genetic deletion of ghrelin decreased food intake. When *ghrl*$^{-/-}$ mice were fed standard chow, we did not observe any significant differences in the cumulative food intake over 10 weeks between male *ghrl*$^{-/-}$ and *ghrl*$^{+/+}$ littermates (Fig. 1B). In addition, there were no significant differences in feeding patterns between *ghrl*$^{+/+}$ and *ghrl*$^{-/-}$ littermates, despite measurement of food intake every 15 min over 11 days using the K2-CABIN apparatus (Fig. 2A). *Ghrl*$^{-/-}$ mice ate higher quantities of food in dark phase than in light phase, which was similar to *ghrl*$^{+/+}$ littermates (Fig. 2B). These results indicate that ghrelin does not have an essential role in feeding patterns.

3.3. Adaptation capability to negative energy states of *ghrl*$^{-/-}$ mice

If ghrelin is necessary for the feeding behaviors induced by negative energy state, *ghrl*$^{-/-}$ mice may exhibit abnormal behaviors during scheduled feeding. Within one week, *ghrl*$^{+/+}$ and *ghrl*$^{-/-}$ littermates both adapted to scheduled feedings, consuming the same amount of food per day (Fig. 3). There were also no differences in water intake or body weight between the

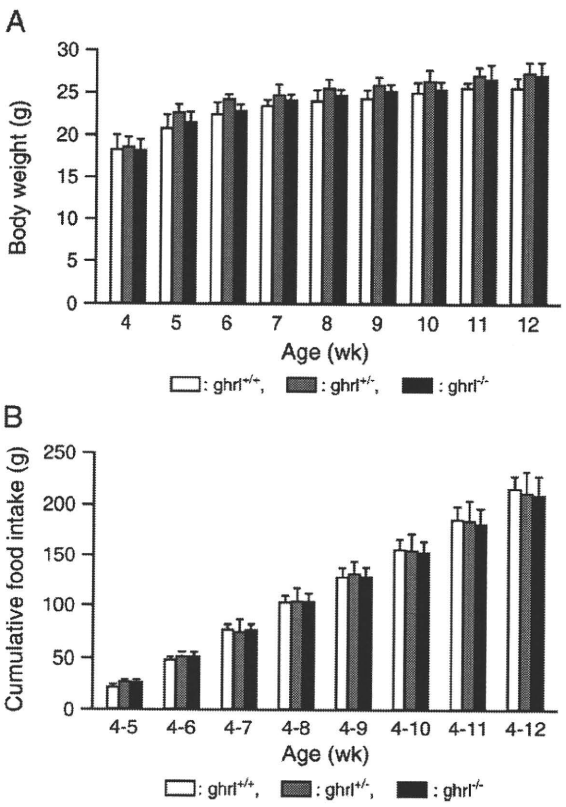

Fig. 1. *Ghrl*$^{-/-}$ mice exhibit normal growth rates and food intake. (A) Body weight; (B) cumulative food intake. Mice were four weeks old at the beginning of the study (n=8, P>0.05 [*ghrl*$^{+/+}$, *ghrl*$^{+/-}$ versus *ghrl*$^{-/-}$ mice]).

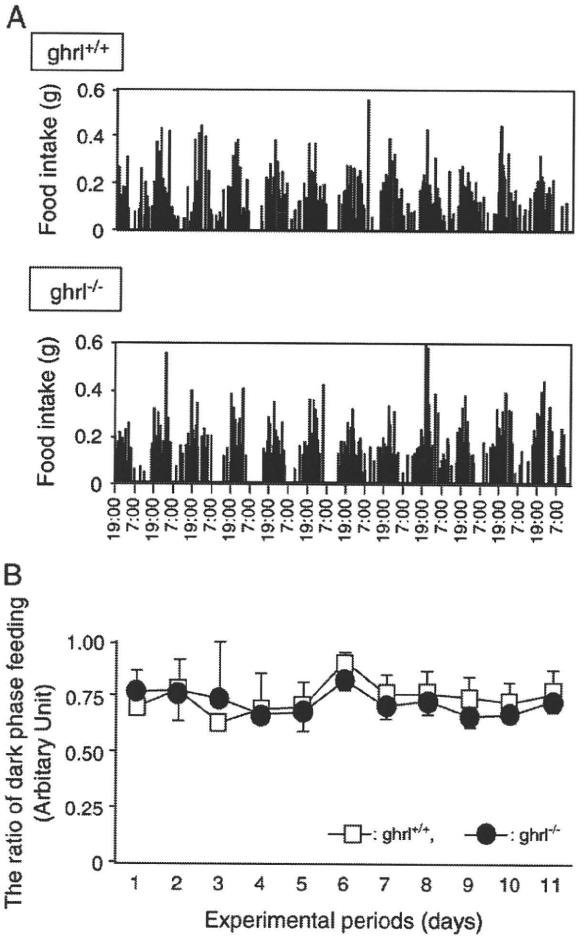

Fig. 2. *Ghrl*$^{-/-}$ mice display normal feeding patterns. (A) Food intake was recorded every 15 min for 11 days; (B) The ratio of dark phase feeding to total feeds (n=6, P>0.05 [*ghrl*$^{+/+}$ versus *ghrl*$^{-/-}$ mice]).

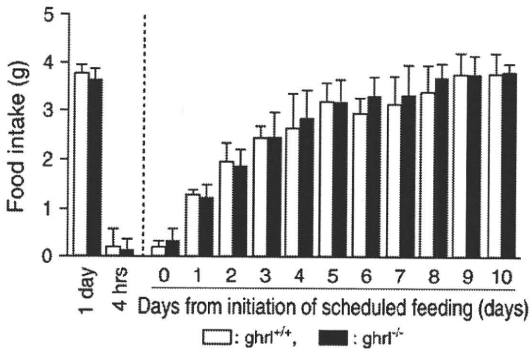

Fig. 3. The adaptation capability of *ghrl*$^{-/-}$ mice to a negative energy state is also normal (n=6, P>0.05 [*ghrl*$^{+/+}$ versus *ghrl*$^{-/-}$ mice]).

two groups (data not shown). These results demonstrate that *ghrl*$^{-/-}$ mice can adapt to a negative energy state.

3.4. Memory-related feeding performances of *ghrl*$^{-/-}$ mice

To test the physiologic role of ghrelin in feeding memory, we performed a food search test. Low values in *ghrl*$^{-/-}$ mice in comparison to *ghrl*$^{+/+}$ mice would indicate a critical role for ghrelin in this process. To test this assumption, we used a novel apparatus called KUROBOX. This apparatus has four food stations, named regions of interest (ROI), in the four corners of the cage (Fig. 4A). At any one time, however, the mouse can only take powder food from a single station. The correct food station rotated counter-clockwise every 4 h. To analyze the food searching behavior of mice, we used the correct visit ratio. This index is the ratio of visits to the correct ROI to the number of visits to all ROIs. In this experiment, the correct visit ratio was the same for *ghrl*$^{-/-}$ mice as that observed for *ghrl*$^{+/+}$ littermates; this index increased with time in both groups (Fig. 4B). Thus, *ghrl*$^{-/-}$ mice did not exhibit impaired feeding memory.

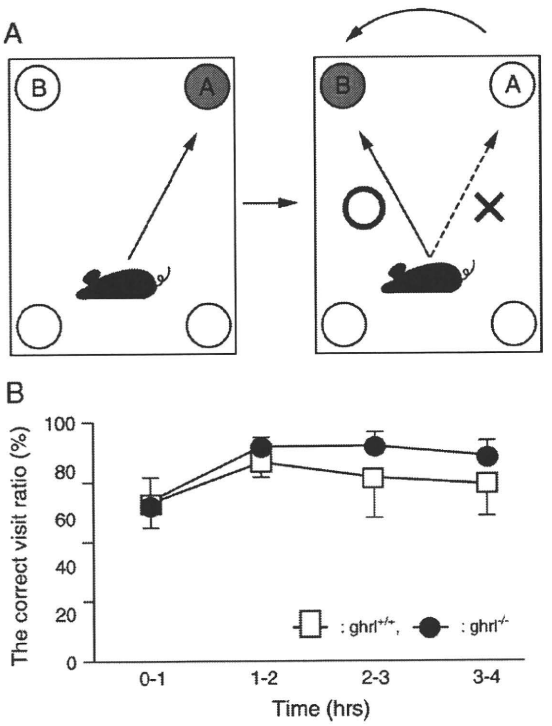

Fig. 4. The memory of feeding in *ghrl*$^{-/-}$ mice is normal. (A) Schematic illustration of the principles of KUROBOX analysis. When feed is first put in ROI A, the mouse always goes to ROI A to eat. Immediately after transferring feeds from ROI A to B, however, the mouse goes to ROI A by mistake at first. Gradually, the mouse goes to the correct ROI B. Investigation of the way of access can help estimate memory tasks in these mice. (B) The correct visit ratio is defined as the ratio of the number of visits to the correct food station to the number of visits to all stations ($n=6$, $P>0.05$ [*ghrl*$^{+/+}$ versus *ghrl*$^{-/-}$ mice]).

4. Discussion

Ghrelin has effects on puberty onset and pregnancy outcomes in rats [11]. Ghrelin also modulates rat testicular function and regulates gonadotropin secretion [12–14]. *Ghrl*$^{-/-}$ mice, however, were fertile and delivered normal litter sizes, indicating that ghrelin is not essential for reproductive function. While a number of reports indicate that ghrelin induces cell proliferation [15–17], there were no gross differences in tissue weights or body weights between *ghrl*$^{+/+}$ *and ghrl*$^{-/-}$ mice. There were no physical or tissue abnormalities identified in *ghrl*$^{-/-}$ mice by our routine analytical protocols. These results suggested that ghrelin is not critical for cell proliferation.

Centrally- or peripherally-injected ghrelin induces acute food intake in rats [18,19]. Ghrelin receptors localize in the SCN and the Arc, important regions in the regulation of circadian rhythms and feeding, respectively [4], suggesting that ghrelin maybe involved in feeding initiation and patterns. *Ghrl*$^{-/-}$ mice, however, have normal feeding patterns, with high food intake in dark phase and low intake in light phase. These results indicate that ghrelin is neither an initiator of feeding nor a regulator of feeding patterns. Ghrelin may act on the SCN to play an unknown role(s) in feeding patterns.

Fasting induces ghrelin secretion from the hypothalamus and stomach in rats [3]. Negative energy states induced by centrally-administered 2-deoxy-D-glucose also stimulates ghrelin secretion from the rat hypothalamus [3]. Plasma ghrelin levels are increased in anorexia nervosa patients and returns to basal levels following weight gain and recovery in these patients [20]. Patients with chronic heart failure (CHF) or chronic obstructive pulmonary disease (COPD) often exhibit a degree of cachexia. Plasma ghrelin levels were significantly higher in CHF patients with cachexia than those without cachexia [21]. Similarly, plasma ghrelin was elevated in underweight patients with COPD, in whom the levels were associated with a cachectic state [22]. Thus, ghrelin secretion is induced by negative energy states, suggesting that ghrelin is necessary for adaptation to negative energy states. In both *ghrl*$^{+/+}$ and *ghrl*$^{-/-}$ mice, however, the capacity to adapt to scheduled feeding was normal. Mice in both groups required approximately one week to eat the same amount of food during over one day. Thus, the absence of ghrelin does not physiologically change the scheduled feedings of mice.

Recently, ghrelin was shown to control hippocampal spine synapse density and memory performance [23]. Therefore, we investigated the memory-related feeding performance of *ghrl*$^{-/-}$ mice using the KUROBOX apparatus. This powerful tool allows us to analyze the memory of feeding. We could not, however, observe any differences in memory-related feeding performance between *ghrl*$^{+/+}$ and *ghrl*$^{-/-}$ mice. In both groups, the correct visit ratio increased with time after transfer of feedings. This result indicates that ghrelin does not control the food searching behaviors or the memory of feeding.

In summary, we did not observe any changes in the feeding performances of *ghrl*$^{-/-}$ mice in this study. Multiple previous reports have demonstrated that ghrelin has an important role in feeding regulation. Therefore, we cannot exclude the possibility that compensatory mechanisms may work to regulate feeding in

ghrl$^{-/-}$ mice. Although we also investigated the gene expression of a subset of orexigenic and anorexigenic peptides, we did not observe any differences between the two groups. It remains possible that an unknown mechanism regulates feeding. Thus, this study demonstrates that ghrelin is not critically required for feeding performance. Further studies will be needed to reveal the essential role(s) of ghrelin in these animals.

Acknowledgments

We thank Y. Yamashita and Y. Yoshida (Kurume University), and A. Kawai and Y. Maruyama (Osaka University) for their helpful assistance.

The studies in the authors' laboratory are supported by grants from Research on Measures for Intractable Diseases from the Health and Labour Sciences Research Grants, the MEXT Open Research Center Project (2004). And this work was supported in part by the Promotion of Basic Research Activities for Innovative Biosciences (PROBRAIN) (to M.K.), by Grant-in-Aids for Scientific Research from the Ministry of Education, Culture, Sports, Science and Technology of Japan (to M.K.), by Kato Memorial Bioscience Foundation (to T.S.), by The Foundation for Growth Science (to T.S.), and by the Sasakawa Scientific Research Grant (to T.S).

References

[1] Kojima M, Hosoda H, Date Y, Nakazato M, Matsuo H, Kangawa K. Ghrelin is a growth-hormone-releasing acylated peptide from stomach. Nature 1999;402:656–60.

[2] Dezaki K, Yada T. Ghrelin in the regulation of glucose and lipid metabolism. Nippon Rinsho 2004;62(Suppl 9):388–91.

[3] Sato T, Fukue Y, Teranishi H, Yoshida Y, Kojima M. Molecular forms of hypothalamic ghrelin and its regulation by fasting and 2-deoxy-D-glucose administration. Endocrinology 2005;146:2510–6.

[4] Zigman JM, Jones JE, Lee CE, Saper CB, Elmquist JK. Expression of ghrelin receptor mRNA in the rat and the mouse brain. J Comp Neurol 2006;494:528–48.

[5] Kamegai J, Tamura H, Shimizu T, Ishii S, Sugihara H, Wakabayashi I. Chronic central infusion of ghrelin increases hypothalamic neuropeptide Y and agouti-related protein mRNA levels and body weight in rats. Diabetes 2001;50:2438–43.

[6] Goto M, Arima H, Watanabe M, Hayashi M, Banno R, Sato I, et al. Ghrelin increases neuropeptide Y and agouti-related peptide gene expression in the arcuate nucleus in rat hypothalamic organotypic cultures. Endocrinology 2006;147:5102–9.

[7] Toshinai K, Date Y, Murakami N, Shimada M, Mondal MS, Shimbara T, et al. Ghrelin-induced food intake is mediated via the orexin pathway. Endocrinology 2003;144:1506–12.

[8] Cowley MA, Cone RD, Enriori P, Louiselle I, Williams SM, Evans AE. Electrophysiological actions of peripheral hormones on melanocortin neurons. Ann N Y Acad Sci 2003;994:175–86.

[9] Sato T, Yamaguchi T, Matsuzaki M, Satoh T, Suzuki A. Mammosomatotrophs develop within mammotroph clusters in bovine adenohypophysis. Tissue Cell 1999;31:499–504.

[10] Kurokawa M, Fujimura K, Sakurai-Yamashita Y. A new-generation apparatus for studying memory-related performance in mice. Cell Mol Neurobiol 2003;23:121–9.

[11] Fernandez-Fernandez R, Navarro VM, Barreiro ML, Vigo EM, Tovar S, Sirotkin AV, et al. Effects of chronic hyperghrelinemia on puberty onset and pregnancy outcome in the rat. Endocrinology 2005;146:3018–25.

[12] Furuta M, Funabashi T, Kimura F. Intracerebroventricular administration of ghrelin rapidly suppresses pulsatile luteinizing hormone secretion in ovariectomized rats. Biochem Biophys Res Commun 2001;288:780–5.

[13] Tena-Sempere M. Ghrelin: novel regulator of gonadal function. J Endocrinol Invest 2005;28:26–9.

[14] Tena-Sempere M, Barreiro ML, Gonzalez LC, Gaytan F, Zhang FP, Caminos JE, et al. Novel expression and functional role of ghrelin in rat testis. Endocrinology 2002;143:717–25.

[15] Kim SW, Her SJ, Park SJ, Kim D, Park KS, Lee HK, et al. Ghrelin stimulates proliferation and differentiation and inhibits apoptosis in osteoblastic MC3T3-E1 cells. Bone 2005;37:359–69.

[16] Nanzer AM, Khalaf S, Mozid AM, Fowkes RC, Patel MV, Burrin JM, et al. Ghrelin exerts a proliferative effect on a rat pituitary somatotroph cell line via the mitogen-activated protein kinase pathway. Eur J Endocrinol 2004;151:233–40.

[17] Duxbury MS, Waseem T, Ito H, Robinson MK, Zinner MJ, Ashley SW, et al. Ghrelin promotes pancreatic adenocarcinoma cellular proliferation and invasiveness. Biochem Biophys Res Commun 2003;309:464–8.

[18] Nakazato M, Murakami N, Date Y, Kojima M, Matsuo H, Kangawa K, et al. A role for ghrelin in the central regulation of feeding. Nature 2001;409:194–8.

[19] Date Y, Murakami N, Toshinai K, Matsukura S, Niijima A, Matsuo H, et al. The role of the gastric afferent vagal nerve in ghrelin-induced feeding and growth hormone secretion in rats. Gastroenterology 2002;123:1120–8.

[20] Cuntz U, Fruhauf E, Wawarta R, Tschop M, Folwaczny C, Riepl R, et al. A role for the novel weight-regulating hormone ghrelin in anorexia nervosa. Am Clin Lab 2002;21:22–3.

[21] Nagaya N, Uematsu M, Kojima M, Date Y, Nakazato M, Okumura H, et al. Elevated circulating level of ghrelin in cachexia associated with chronic heart failure: relationships between ghrelin and anabolic/catabolic factors. Circulation 2001;104:2034–8.

[22] Itoh T, Nagaya N, Yoshikawa M, Fukuoka A, Takenaka H, Shimizu Y, et al. Elevated plasma ghrelin level in underweight patients with chronic obstructive pulmonary disease. Am J Respir Crit Care Med 2004;170:879–8782.

[23] Diano S, Farr SA, Benoit SC, McNay EC, da Silva I, Horvath B, et al. Ghrelin controls hippocampal spine synapse density and memory performance. Nat Neurosci 2006;9:381–8.

Research Article

The Polycomb Gene Product BMI1 Contributes to the Maintenance of Tumor-Initiating Side Population Cells in Hepatocellular Carcinoma

Tetsuhiro Chiba,[1,4] Satoru Miyagi,[1] Atsunori Saraya,[1] Ryutaro Aoki,[1] Atsuyoshi Seki,[1] Yohei Morita,[3] Yutaka Yonemitsu,[2] Osamu Yokosuka,[2] Hideki Taniguchi,[5] Hiromitsu Nakauchi,[3] and Atsushi Iwama[1,4]

[1]Department of Cellular and Molecular Medicine and [2]Department of Medicine and Clinical Oncology, Graduate School of Medicine, Chiba University, Chiba, Japan; [3]Laboratory of Stem Cell Therapy, Center for Experimental Medicine, University of Tokyo; [4]JST, CREST, Tokyo, Japan; and [5]Department of Regenerative Medicine, Graduate School of Medical Science, Yokohama City University, Yokohama, Japan

Abstract

Side population (SP) cell analysis and sorting have been successfully applied to hepatocellular carcinoma (HCC) cell lines to identify a minor cell population with cancer stem cell properties. However, the molecular mechanisms operating in SP cells remain unclear. The polycomb gene product BMI1 plays a central role in the self-renewal of somatic stem cells in a variety of tissues and organs and seems to be implicated in tumor development. In this study, we determined the critical role of BMI1 in the maintenance of cancer stem cells with the SP phenotype in HCC cell lines. BMI1 was preferentially expressed in SP cells in Huh7 and PLC/PRF/5 HCC cells compared with the corresponding non-SP cells. Lentiviral knockdown of *BMI1* considerably decreased the number of SP cells in both Huh7 and PLC/PRF/5 cells. Long-term culture of purified SP cells resulted in a drastic reduction in the SP subpopulation upon the *BMI1* knockdown, indicating that BMI1 is required for the self-renewal of SP cells in culture. More importantly, the *BMI1* knockdown abolished the tumor-initiating ability of SP cells in nonobese diabetic/severe combined immunodeficiency mice. Derepression of the *INK4A* and *ARF* genes that are major targets for BMI1 was not necessarily associated with impaired self-renewal of SP cells caused by *BMI1* knockdown. In conclusion, our findings define an important role for BMI1 in the maintenance of tumor-initiating SP cells in HCC. BMI1 might be a novel therapeutic target for the eradication of cancer stem cells in HCC. [Cancer Res 2008;68(19):7742–9]

Introduction

According to the recent "cancer stem cell hypothesis," tumors consist of a minor component of tumorigenic cells and a major component of nontumorigenic cells (1, 2). The minor population, termed cancer stem cells or tumor-initiating cells, construct a hierarchical structure containing varied descendants in a similar fashion to the normal stem cell systems and possesses a prominent ability to initiate new tumors in xenograft transplantation (3, 4). In addition, these cells seem to be highly resistant to traditional forms of anticancer therapy such as chemotherapy and radiotherapy (5, 6), resulting in residual cancer stem cells which, in many instances, lead to the recurrence of the cancer (7). Therefore, an overall understanding of the various biological aspects of cancer stem cells is of paramount importance to both the elucidation of mechanisms underlying carcinogenesis and the establishment of novel therapeutic strategies.

Side population (SP) cell analysis and sorting were initially used for the isolation of hematopoietic stem cells in bone marrow cells (8). Currently, they are widely applied to the enrichment of putative normal stem cells in a variety of tissues and organs (9–11). The SP phenotype is determined by the ability to efflux the Hoechst 33342 dye through an ATP-binding cassette (ABC) membrane transporter. Of note, recent studies showed that SP cells isolated from diverse cancer cell lines harbor stem cell–like properties (12–14). Given that many different types of cancer cells frequently show overexpression of ABC transporters and exhibit drug resistance (15), it is quite reasonable to detect stem-like fractions in cancer cells using this approach. We previously applied SP analysis and sorting to established hepatocellular carcinoma (HCC) cell lines and found that in Huh7 and PLC/PRF/5 cells, SP fractions made up <1% of the total cell population (12). As expected, the SP subpopulations showed cancer stem cell–like properties both in culture and in an *in vivo* transplant model. These stem cell biology-based strategies enabled us to perform further analyses.

We and others previously reported that the polycomb-group (PcG) gene *Bmi1* plays a critical role in the self-renewal of a range of somatic stem cells, including hepatic stem cells, based on gain-of-function and loss-of-function analyses (16, 17). It seems likely that both normal and cancer stem cells share not only a number of surface marker phenotypes but also a list of molecular mechanisms for self-renewal and differentiation. This has been well shown in the leukemic stem cell system (18–20), although little is known in solid cancers.

In the current study, we examined the crucial role of BMI1 in the maintenance of the tumor-initiating SP subpopulation in HCC cells. Taking advantage of lentivirus-mediated knockdown and retrovirus-mediated overexpression techniques, we examined whether BMI1 regulates the self-renewal and differentiation of SP cells in culture and their tumorigenicity in a nonobese diabetic/severe combined immunodeficient (NOD/SCID) xenograft transplant model.

Note: Supplementary data for this article are available at Cancer Research Online (http://cancerres.aacrjournals.org/).

Requests for reprints: Atsushi Iwama, Department of Cellular and Molecular Medicine, Graduate School of Medicine, Chiba University, 1-8-1 Inohana, Chu-ku, Chiba 260-8670, Japan. Phone: 81-43-2262189; Fax: 81-43-2262191; E-mail: aiwama@faculty.chiba-u.jp.

doi:10.1158/0008-5472.CAN-07-5882

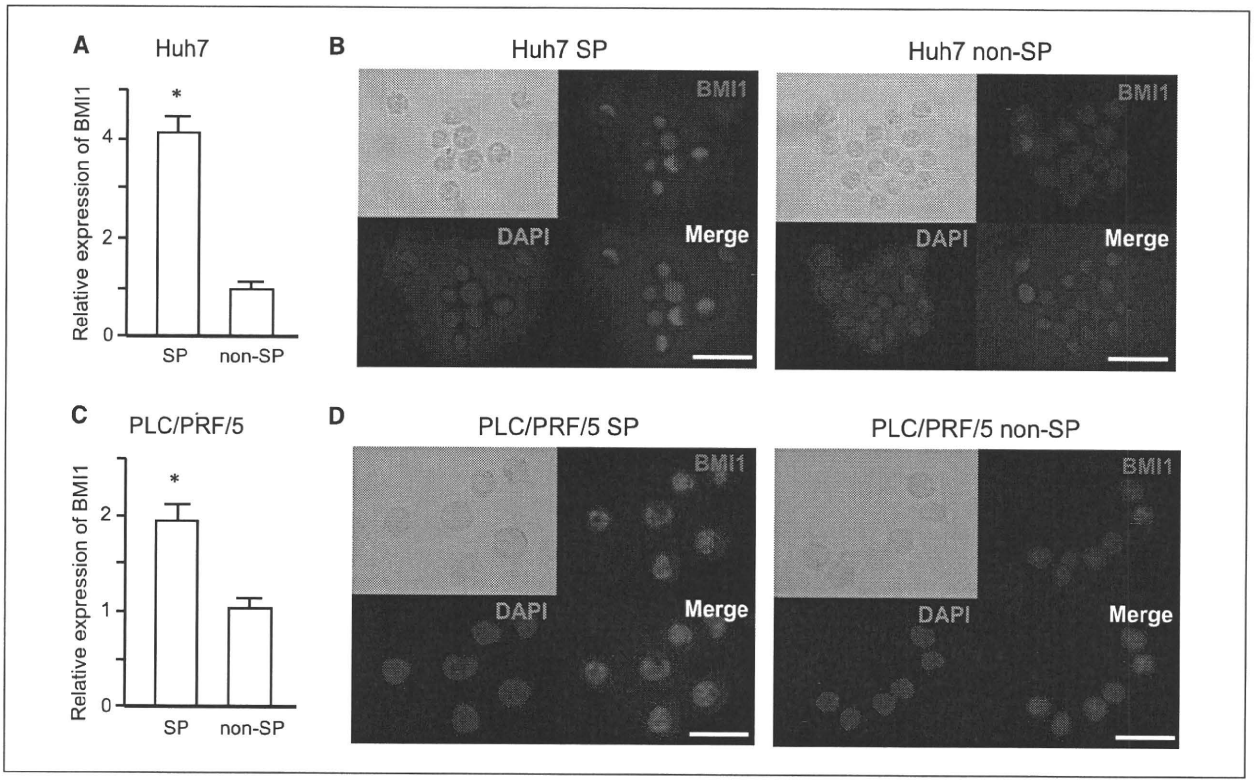

Figure 1. Expression of BMI1 in SP and non-SP cells. Real-time RT-PCR analyses of *BMI1* expression in SP and non-SP cells from Huh7 (*A*) and PLC/PRF/5 cells (*C*). Immunocytochemical analyses of BMI1 expression in SP and non-SP cells from Huh7 (*B*) and PLC/PRF/5 cells (*D*). Nuclear DAPI staining (*blue*) and immunofluorescent labeling of BMI1 (*red*) are merged. *, statistically significant ($P < 0.05$). *Scale bar*, 50 μm.

Materials and Methods

Mice. NOD/SCID mice were purchased from Sankyo Laboratory Co. Ltd. They were bred and maintained in accordance with our institutional guidelines for the use of laboratory animals.

Cell culture. The human liver cancer cell lines Huh7 and PLC/PRF/5 were cultured in DMEM (Invitrogen Life Technologies) containing 10% FCS and 1% penicillin/streptomycin (Invitrogen).

Flow cytometry. SP analysis and sorting were performed, as described previously (12). Briefly, the suspended cells were incubated at 37°C for 90 min with 20 μg/mL Hoechst 33342 (Sigma Chemical), either alone or in the presence of 50 μmol/L verapamil (Sigma). For the analysis of CD133 expression, cells were incubated with phycoerythrin-conjugated CD133/1 (Miltenyi Biotec). Propidium iodide (BD PharMingen) was added for the elimination of dead cells. Cell analysis and sorting were performed using MoFlo (DakoCytomation).

Immunocytochemistry. Freshly isolated SP cells and non-SP cells were placed on poly-L-lysine–coated slide glasses. After fixation with 2% paraformaldehyde and blocking in 10% goat serum, the cells were incubated with 0.5% Triton-X in PBS for 20 min at room temperature. After incubation, the cells were stained with a primary antibody, anti-Bmi1 (F6; Upstate Biotechnology), at a dilution of 1:200 for 12 h at 4°C. The cells then were washed and incubated with Alexa-555–conjugated goat anti-mouse IgG (Molecular Probes) at a dilution of 1:500 for 2 h at room temperature. After being washed in PBS, the cells were coverslipped with a mounting medium containing 4′,6-diamidino-2-phenylindole (DAPI; Vector Laboratories).

Viral production and transduction. Lentiviral vectors (CS-H1-shRNA-EF-1α-EGFP) expressing short hairpin RNA (shRNA) that targets human *BMI1* (target sequence: sh-*BMI1*-1, 5′-CAGATGAAGATAAGAGAAT-3′; sh-*BMI1*-2, 5′-GAGAAGGAATGGTCCACTT-3′) and *luciferase* were constructed. Human *BMI1* cDNA (a kind gift from Dr. Kazuhito Yamamoto) was cloned into a site upstream of IRES–enhanced green fluorescent protein (EGFP) in the pMCs-IG retroviral vector (21). Recombinant lentiviruses and retroviruses were produced as described before (17, 22).

Western blotting. Cells transduced with the indicated viruses were selected by cell sorting for EGFP expression and subjected to Western blot analysis using anti-Bmi1 (F6) and anti–α-tubulin (Ab-1; Oncogene Science) antibodies.

Reverse transcription–PCR. Total RNA extraction and cDNA synthesis were conducted, as described previously (12). Real-time PCR was performed using TaqMan technology and the ABI PRISM 7000 Sequence Detection System (Applied Biosystems). TaqMan probe and primers for *BMI1* (assay ID Hs00180411_m1) and *β-actin* (assay ID Hs99999903_m1) were obtained from TaqMan gene expression assays (Applied Biosystems). To examine the mRNA expression of *INK4A/ARF* genes in SP cells following *BMI1* knockdown, multiplex reverse transcription–PCR (RT-PCR) was performed as described previously (23). PCR for *BMI1* and *β-actin* was conducted using the following primers: *BMI1* (forward 5′-AGC AGC AAT GAC TGT GAT GC-3′, reverse 5′-CAG TCT CAG GTA TCA ACC AG-3′), *β-actin* (forward 5′-ATC CTG CGT CTG GAC CTG GCT GG-3′, reverse 5′-ACA TGC CGG AGC CGT TGT CGA CGA-3′).

Xenograft transplantation. Various numbers of SP and non-SP cells stably expressing shRNA against *BMI1* or *luciferase* were suspended in DMEM and Matrigel (Becton Dickinson; 1:1) and transplanted to NOD/SCID mice (male, 6–10 wk) under anesthesia. *BMI1* knockdown cells and control cells were implanted into the s.c. space on the right and left sides of the back of recipient mice, respectively. To examine whether enforced expression of *BMI1* in SP cells promotes tumorigenesis, 1×10^4 Huh7 SP cells transduced with *BMI1* and *EGFP* retroviruses were also transplanted.

Tumor formation was observed weekly for 14 wk. The transplantation assays were performed in accordance with institutional guidelines for the use of laboratory animals.

Immunohistochemical analysis. The subcutaneous tumors formed in NOD/SCID mice were fixed in formalin and embedded in paraffin. The sections were subjected to H&E staining. For dual immunohistochemical analyses, the sections were stained with anti-EGFP (BD Biosciences Clontech) and anti-BMI1 (F6), followed by incubation with Alexa-488–conjugated goat anti-rabbit IgG and Alexa-555–conjugated goat anti-mouse IgG (Molecular Probes), respectively.

Statistical analysis. Data are presented as the means ± SE. Statistical differences between two groups were analyzed using the Mann-Whitney units test. P values <0.05 were considered significant.

Results

Preferential expression of BMI1 in SP cells. To gain insight into the crucial role of the polycomb gene product BMI1, we first examined the basal expression of BMI1 in the SP population in Huh7 and PLC/PRF/5 cells. Real-time RT-PCR analyses showed that the mRNA expression of *BMI1* was 4.10 ± 0.36-fold and 1.92 ± 0.25-fold higher in Huh7 and PLC/PRF/5 SP cells than in the corresponding non-SP cells, respectively (Fig. 1*A* and *C*). Immunocytochemical analyses confirmed that BMI1 is highly expressed in the nuclei of SP cells rather than the corresponding non-SP cells in both cell lines (Fig. 1*B* and *D*).

Stable knockdown of *BMI1* by shRNA. We next performed loss-of-function analyses of BMI1 *in vitro*. Stable knockdown of *BMI1* in Huh7 and PLC/PRF/5 cells was achieved by lentivirus-mediated delivery of shRNA against *BMI1*. A lentiviral vector expressing shRNA against *luciferase* was used as a control. We obtained stable cell lines expressing shRNA against *BMI1* or *luciferase* by cell sorting using EGFP as a marker for infection. Western blot analysis showed that both sh-*BMI1*-1 and sh-*BMI1*-2 markedly repressed BMI1 expression in both cell lines, although sh-*BMI1*-1 was less effective than sh-*BMI1*-2 (Fig. 2*A*). Both shRNA inhibited the growth of HCC cell lines. In good agreement with the Western blot data, sh-*BMI1*-2 was more effective in growth suppression than sh-*BMI1*-1 (Fig. 2*B* and *C*). The viability of cells expressing shRNA against *BMI1* was comparable with that of control cells (data not shown).

Detection and isolation of SP cells. SP cell analysis and sorting were performed in Huh7 and PLC/PRF/5 cells stably expressing shRNA against *BMI1* (Fig. 3 and Supplementary Fig. S1). *BMI1* knockdown using sh-*BMI1*-2 considerably decreased the size of the SP population from 0.67 ± 0.09% to 0.19 ± 0.03% in Huh7 cells and from 0.87 ± 0.10% to 0.40 ± 0.04% in PLC/PRF/5 cells (Fig. 3). On the other hand, *BMI1* knockdown using sh-*BMI1*-1 slightly decreased the percentage of SP cells from 0.59 ± 0.04% to 0.32 ± 0.03% in Huh7 cells and from 0.82 ± 0.06% to 0.47 ± 0.03% in PLC/PRF/5 cells (Supplementary Fig. S1). The SP population showed a drastic reduction in number on treatment with the calcium channel blocker verapamil.

Stable overexpression of *BMI1* by retroviral vector. Next, we tested the overexpression of *BMI1* in HCC cells (Supplementary Fig. S2*A*). In clear contrast with the knockdown experiment, the SP subpopulation increased nearly 8-fold with the overexpression of *BMI1* in Huh7 cells (Supplementary Fig. S2*B*). Next, we examined the tumorigenicity of Huh7 SP cells transduced with *BMI1* in NOD/SCID xenograft transplantation. The implantation of 1×10^4 SP cells transduced with *BMI1* resulted in early onset and aggressive

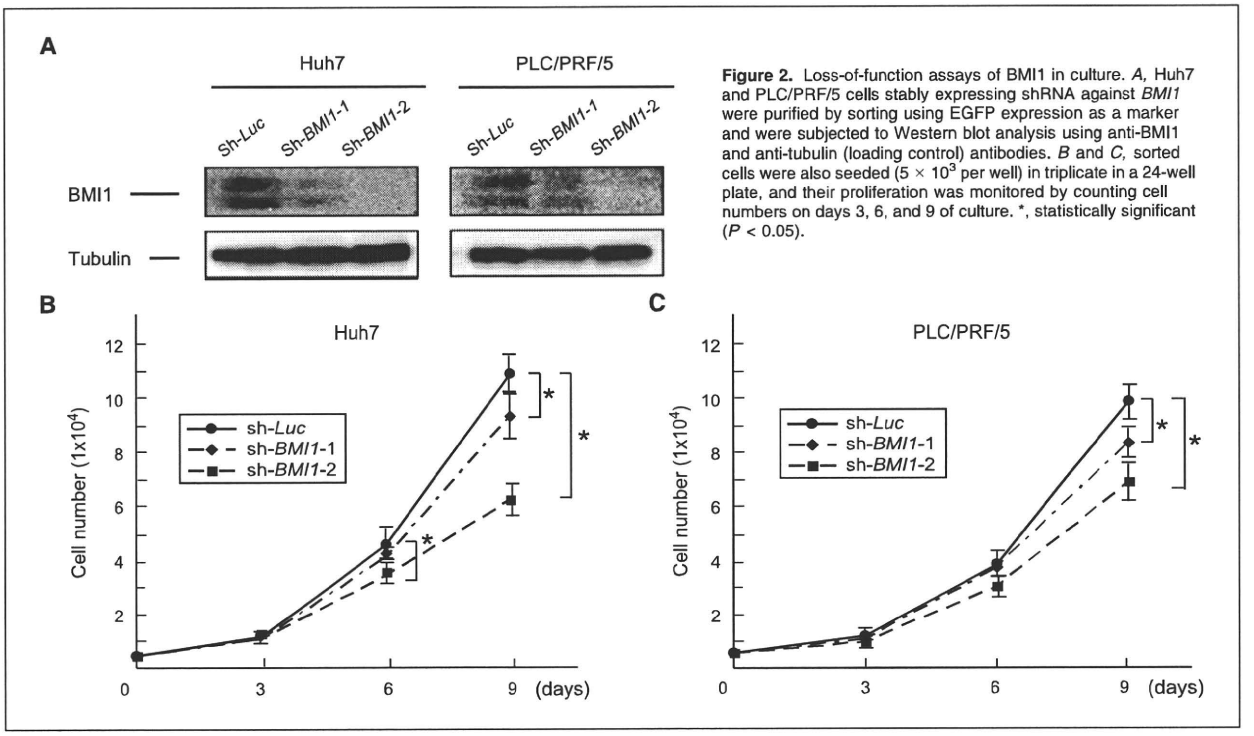

Figure 2. Loss-of-function assays of BMI1 in culture. *A*, Huh7 and PLC/PRF/5 cells stably expressing shRNA against *BMI1* were purified by sorting using EGFP expression as a marker and were subjected to Western blot analysis using anti-BMI1 and anti-tubulin (loading control) antibodies. *B* and *C*, sorted cells were also seeded (5×10^3 per well) in triplicate in a 24-well plate, and their proliferation was monitored by counting cell numbers on days 3, 6, and 9 of culture. *, statistically significant ($P < 0.05$).

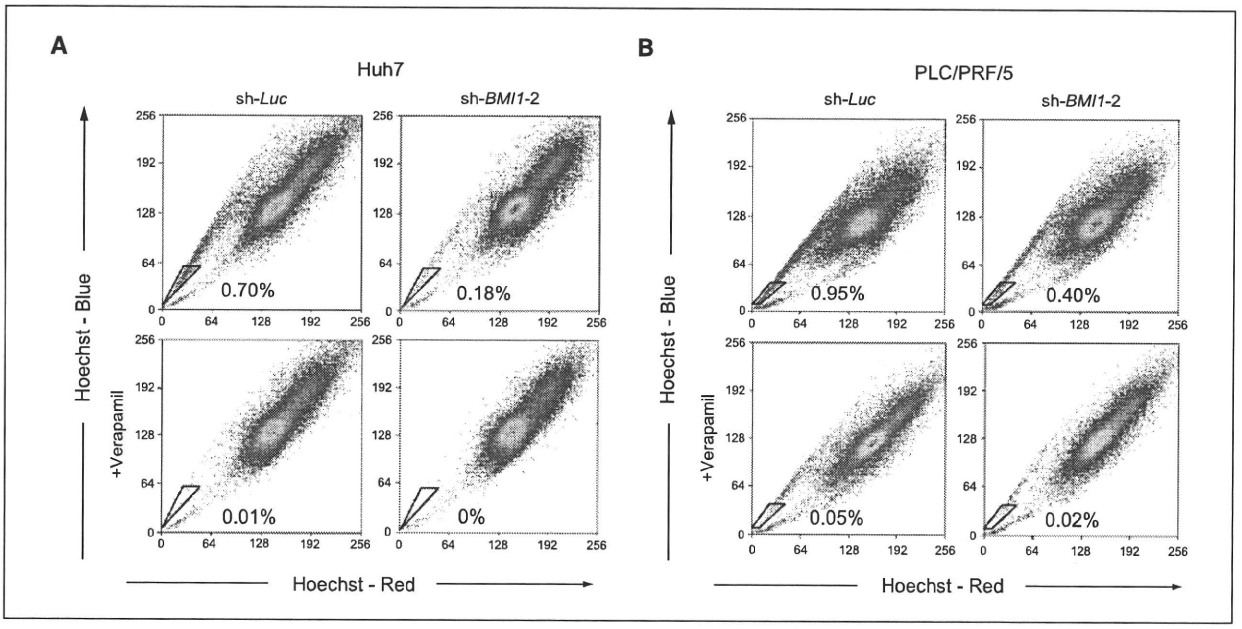

Figure 3. SP cell analysis in *BMI1* knockdown HCC cells by sh-*BMI1*-2. Flow cytometric profiles of SP cells among Huh7 (*A*) and PLC/PRF/5 cells (*B*) after stable knockdown of *BMI1* by sh-*BMI1*-2. SP cell profiles in the presence of verapamil are depicted at the bottom. The percentages of SP cells are indicated.

tumor growth compared with that of control SP cells expressing EGFP (Supplementary Fig. S2*C* and *D*). These results indicated that forced expression of *BMI1* leads to not only enhanced self-renewal but also increased tumorigenicity of SP cells.

Expression of the *INK4A/ARF* gene in *BMI1* knockdown SP cells. To address whether the knockdown of *BMI1* causes derepression of the *INK4A* and *ARF* genes as observed in *Bmi1*-deficient hematopoietic stem cells (HSC; ref. 17), we examined their mRNA expression in SP cells freshly isolated from *BMI1* knockdown and control cells (Fig. 4*A*). In Huh7 SP cells, in which *INK4A* expression is repressed by aberrant DNA methylation in its promoter region (23) and *ARF* is constitutively expressed, *BMI1* knockdown did not affect their expression at all. Conversely, *BMI1* knockdown in PLC/PRF/5 SP cells, in which both *INK4A* and *ARF* are moderately expressed, greatly augmented their expression.

Reanalysis of isolated SP cells. We have previously reported that purified SP cells self-renew and generate nontumorigenic non-SP cells through asymmetrical cell division *in vivo* (12). Purified SP cells repopulate the same hierarchical structure as the original tumor cells consisting of a minor component of SP cells and a major component of non-SP cells (12, 24). This process occurs both *in vitro* and *in vivo*. The SP cells in repopulated tumor retain the same tumor-initiating capacity as the original SP cells. We purified SP cells from both *BMI1* knockdown and control cells and cultured them for 4 weeks to examine the role of BMI1 in this process in culture. The SP subpopulation in *BMI1* knockdown Huh7 cells profoundly decreased (5.5%) compared with that in the control cells (18.8%; Fig. 4*B*). Likewise, the percentage of PLC/PRF/5 SP cells among *BMI1* knockdown and control cells was 6.1% and 22.0%, respectively (Fig. 4*B*). These results imply that BMI1 regulates the self-renewal capability of tumor-initiating SP cells and loss of BMI1 accelerates differentiation toward nontumorigenic non-SP cells.

The role for BMI1 in the maintenance of tumorigenic CD133-positive Huh7 cells. It has been reported that CD133-positive cells possessed greater tumorigenicity than CD133-negative cells in HCC cells, including Huh7 cells (25). Although the majority of Huh7 cells are CD133-positive (Fig. 4*C*), it has been shown that CD133 expression is stronger in SP cells than in non-SP cells (24). We then evaluated the expression of CD133 in the context of BMI1 expression using flow cytometry. *BMI1* knockdown decreased the CD133-positive fraction from 74.2% to 60.9%, whereas *BMI1* overexpression increased it from 71.6% to 84.4% (Fig. 4*C*). These findings indicate that the expression level of BMI1 is tightly correlated with the cancer stem cell phenotype represented not only by SP cells but also by CD133-positive cells.

Tumorigenic ability in xenograft transplantation. To determine whether loss of BMI1 affects the tumorigenicity *in vivo*, various numbers of SP and non-SP cells sorted from the *BMI1* knockdown or control HCC cells were transplanted into NOD/SCID mice (Fig. 5; Table 1). As few as 1×10^3 control SP cells were enough to initiate tumors for both cell lines. In contrast, 1×10^3 *BMI1* knockdown SP cells transduced with sh-*BMI1*-1 and 1×10^4 *BMI1* knockdown SP cells transduced with sh-*BMI1*-2 from Huh7 and PLC/PRF/5 cells failed to initiate subcutaneous tumors in any recipient mice. Tumors derived from control SP cells showed similar histologic features to those formed by the injection of unsorted cells and exhibited the nuclear expression of BMI1 (Fig. 5). Unexpectedly, 1×10^5 *BMI1* knockdown Huh7 and PLC/PRF/5 SP cells with sh-*BMI1*-2 gave rise to tumors in one of three and one of two mice, respectively. However, the tumor size was less than half that of control SP cells. Furthermore,

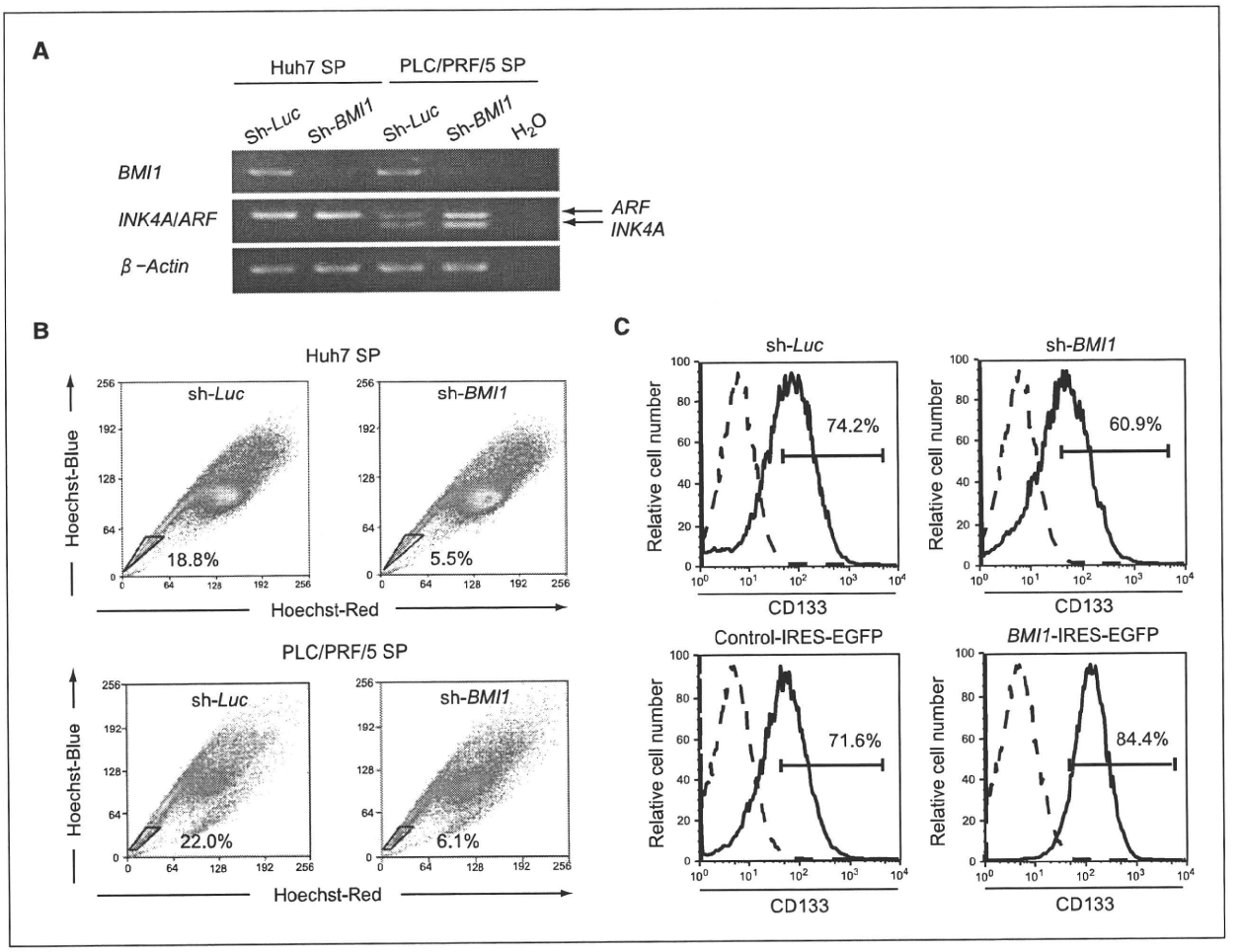

Figure 4. Role of BMI1 in *INK4A/ARF* expression and cancer stem cell phenotype. *A*, RT-PCR analysis of *INK4A/ARF* in *BMI1* knockdown SP cells from Huh7 and PLC/PRF/5 cells. Lane H_2O represents the negative control without the template. *B*, flow cytometric profiles of purified SP cells after culture. SP cells were purified from *BMI1* knockdown cells, cultured for 4 wk, and then subjected to the flow cytometric analysis. *C*, expression of CD133 in *BMI1* knockdown (*top*) and *BMI1* overexpressing cells (*bottom*) detected by flow cytometric analysis. Dotted line represents negative controls. The percentages of CD133-positive cells are indicated.

immunohistochemical analyses revealed that tumors predominantly consisted of contaminating EGFP-negative cells or EGFP-positive cells showing no obvious effects of *BMI1* knockdown (Supplementary Fig. S3). By contrast, tumors derived from control SP cells did not contain EGFP-negative cells at all (Fig. 5). These results further support that the tumor-initiating capacity is profoundly impaired by *BMI1* knockdown. In contrast, the injection of 1×10^6 non-SP cells from either cell line failed to generate tumors in any mice.

Discussion

PcG proteins form chromatin-associated multiprotein complexes, polycomb repressive complex 1 (PRC1) and PRC2 and function as a cellular memory system through epigenetic chromatin modifications (26, 27). Bmi1, a component of PRC1, has been implicated in the regulation of self-renewal in a range of different stem cell systems (28, 29). Of note, Bmi1 is also required for the maintenance of self-renewing leukemic stem cells in a mouse model using *Bmi1*$^{-/-}$ HSCs (30). Recent reports described that BMI1 is preferentially expressed in the tumorigenic subpopulation in breast cancer and head and neck tumors (31, 32). Consistent with these reports, we previously showed that forced expression of *BMI1* promotes the self-renewal of hepatic stem/progenitor cells and contributes to malignant transformation (16). In addition, immunohistochemical analyses showed BMI1 to be overexpressed in >60% of human HCC cases examined.[6] Together, all these findings highlight the importance of BMI1 in hepatocarcinogenesis and implicate BMI1 in the self-renewal of cancer stem cells in HCC.

In the present study, we first examined the basal expression of BMI1 in Huh7 and PLC/PRF/5 SP cells. As expected, both the real-

[6] Unpublished data.

time RT-PCR and immunocytochemical analyses showed BMI1 expression to be stronger in SP cells than non-SP cells in each cell line. We thus directly evaluated the role of BMI1 in cancer stem cell–like SP cells. Lentiviral shRNA-mediated knockdown of *BMI1* allowed a highly efficient loss-of-function assay of the SP subpopulation in culture and in an *in vivo* transplant model. The analysis showed a significant decrease in the frequency of SP cells among the *BMI1* knockdown cells compared with the corresponding control cells. Furthermore, analysis of the growth and differentiation of purified SP cells revealed that loss of BMI1 causes a considerable decrease in the SP subpopulation and facilitates differentiation toward non-SP cells. These results indicated that BMI1 contributes to the self-renewal of SP cells in culture.

Notably, when as few as 1×10^3 control SP cells were sufficient to initiate tumors in NOD/SCID mice, even 10 times more *BMI1* knockdown SP cells (1×10^4) failed to develop tumors. 1×10^5 *BMI1* knockdown SP cells gave increase to tumors in some of the recipient mice, but the tumor-initiating capacity was profoundly reduced. Collectively, the tumorigenic activity in the SP subpopulation seemed to be attenuated nearly 100-fold by the *BMI1* knockdown. Although the important role of Bmi1 in the maintenance of cancer stem cells has already been shown in a mouse leukemia model, this is the first direct evidence that the loss of BMI1 in established cancer stem cells can affect their ability to self-renew and tumorigenicity. The role of BMI1 in the regulation of tumor-initiating SP cells was further supported by the findings of the gain-of-function assay. Although stable knockdown of *BMI1* decreased SP cell numbers *in vitro*, it did not completely abolish SP cells and its effect varied among HCC cell lines. These results strongly indicate that the SP subpopulation is quite heterogeneous, and the contribution of BMI1 to the SP phenotype differs among the cell lines. Considering that BMI1 is just one of multiple self-renewal regulators, the different contributions of molecular machinery, including the Notch, Wnt, and Shh signaling pathways, might also influence the SP phenotype (33). Further analyses would be necessary to clarify the mechanisms underlying the regulation of cancer stem cells in HCC.

Bmi1 regulates the cell cycle, apoptosis and senescence by repressing the *Ink4a/Arf* locus (26, 34). In *Bmi1*-deficient mice, the expression of *Ink4a* and *Arf* is markedly increased in HSCs (17). Conversely, deletion of both *Ink4a* and *Arf* substantially restores the impaired capacity of $Bmi1^{-/-}$ HSCs to self-renew (22). These findings suggest that Bmi1 regulates HSCs by acting as a critical failsafe against the premature loss of HSCs induced by Ink4a and Arf-dependent senescence pathways. On the other hand, the Ink4a-Rb and Arf-p53–dependent cellular senescence pathways play a critical role in the triggering of oncogene-induced senescence, which is of substantial importance to the elimination of transforming cells that potentially develop into cancer stem cells (26, 35). In the present study, the expression of the *INK4A* and *ARF* genes was augmented by *BMI1* knockdown in PLC/PRF/5 cells. In this case, derepression of *INK4A* and *ARF* could account for the impaired self-renewal of PLC/PRF/5 SP cells with *BMI1* knockdown. On the other hand, knockdown of *BMI1* in Huh7 cells resulted in no remarkable changes in *INK4A* and *ARF* gene expression compared with the control. Given that the function of p53 is impeded by mutations in Huh7 cells (36), additional targets for BMI1 other than the *INK4A/ARF* locus might be responsible for

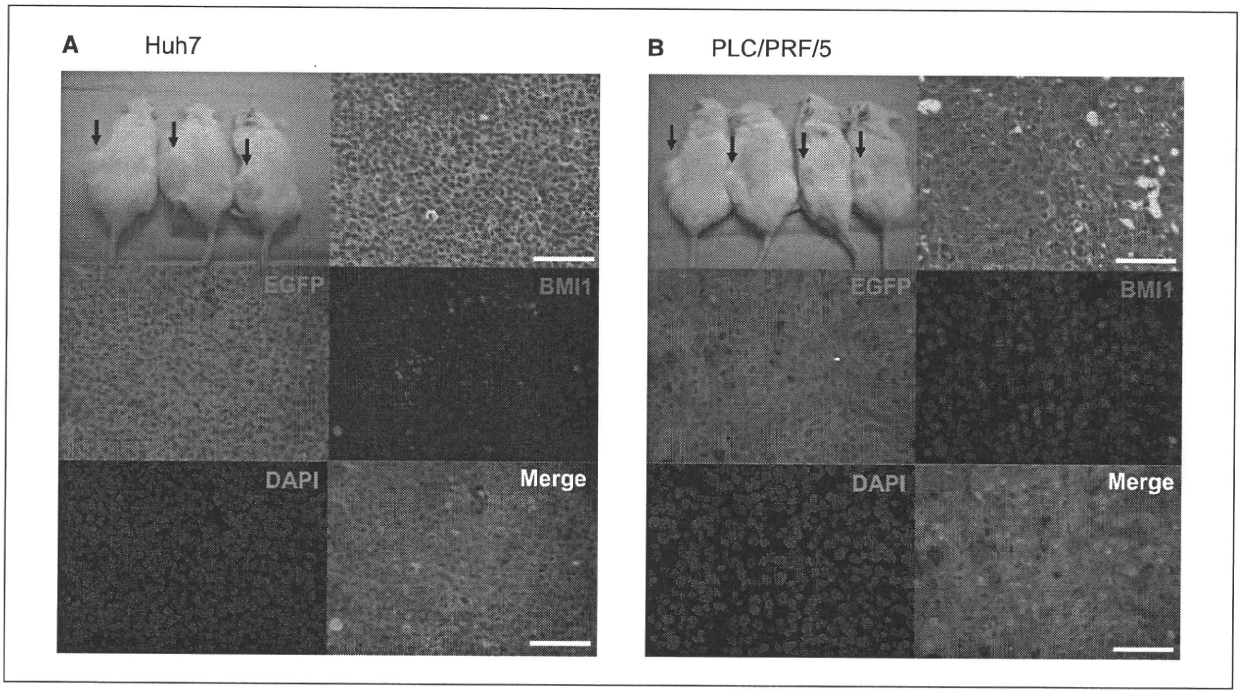

Figure 5. Loss of tumorigenicity in SP cells by *BMI1* knockdown. 1×10^3 control SP cells from Huh7 (*A*) and PLC/PRF/5 cells (*B*) generated tumors in the left subcutaneous space of recipient mice (*arrows*), whereas *BMI1* knockdown SP cells failed to initiate tumors in the right space. Immunohistochemical analyses revealed the nuclear localization of BMI1 in tumor cells generated by control SP cells. *Scale bar*, 100 μm.

Table 1. Tumor-initiating ability of SP cells in the NOD/SCID xenograft transplant model

	No. implanted cells				
	100	1×10^3	1×10^4	1×10^5	1×10^6
Huh7					
sh-*Luc*					
SP cells	0/5	14/15	13/13		
Non-SP cells		0/15	0/14	0/10	0/5
sh-*BMI1*-1					
SP cells	0/5	0/6	3/6*		
Non-SP cells		0/6	0/6	0/5	0/5
sh-*BMI1*-2					
SP cells	0/5	0/9	0/8	1/3†	
Non-SP cells		0/9	0/8	0/5	0/5
PLC/PRF/5					
Sh-*Luc*					
SP cells	0/5	14/14	14/14		
Non-SP cells		0/14	0/14	0/10	0/5
sh-*BMI1*-1					
SP cells	0/5	0/5	2/5*		
Non-SP cells		0/4	0/5	0/5	0/5
sh-*BMI1*-2					
SP cells	0/5	0/9	0/9	1/2†	
Non-SP cells		0/9	0/9	0/5	0/5

NOTE: Tumor initiation was monitored for 14 wk after implantation.
*Delayed tumor formation and a decrease in tumor size were observed compared with tumors derived from control SP cells.
†Immunohistochemical data for tumors are displayed in Supplementary Fig. S3.

the impaired ability of Huh7 SP cells to self-renew. Thus, BMI1 might function in the maintenance of HCC cancer stem cells in both an *INK4A/ARF*-dependent and an *INK4A/ARF*-independent manner.

Finally, the present loss-of-function and gain-of-function assays revealed that BMI1 determines the self-renewal capability of SP cells, which directly contributes to the tumorigenic potential. However, further analysis will definitely be necessary to determine the role of BMI1 in primary HCC cancer stem cells (37). Our findings also indicate BMI1 to be a novel therapeutic target for the eradication of cancer stem cells in HCC. It would be of paramount importance to understand differential functions and targets of BMI1 in normal and cancer stem cells.

Disclosure of Potential Conflicts of Interest

No potential conflicts of interest were disclosed.

Acknowledgments

Received 10/15/2007; revised 7/10/2008; accepted 7/18/2008.

Grant support: Ministry of Education, Culture, Sports, Science and Technology, Japan; Core Research for Evolutional Science and Technology of Japan Science and Technology Corporation; and the Public Trust Haraguchi Memorial Cancer Research Fund and Sagawa Foundation for Promotion for Cancer Research.

The costs of publication of this article were defrayed in part by the payment of page charges. This article must therefore be hereby marked *advertisement* in accordance with 18 U.S.C. Section 1734 solely to indicate this fact.

We thank Drs. Toshio Kitamura (Tokyo University) and Hiroyuki Miyoshi (RIKEN) for providing pMCs-IG and CS-H1-shRNA-EF-1α-EGFP, respectively, Yuji Yamazaki for technical support in flow cytometry and Mieko Tanemura for laboratory assistance.

References

1. Reya T, Morrison SJ, Clarke MF, Weissman IL. Stem cells, cancer, and cancer stem cells. Nature 2001;414:105–11.
2. Jordan CT, Guzman ML, Noble M. Cancer stem cells. N Engl J Med 2006;355:1253–61.
3. Bonnet D, Dick JE. Human acute myeloid leukemia is organized as a hierarchy that originates from a primitive hematopoietic cell. Nat Med 1997;3:730–7.
4. Al-Hajj M, Wicha MS, Benito-Hernandez A, Morrison SJ, Clarke MF. Prospective identification of tumorigenic breast cancer cells. Proc Natl Acad Sci U S A 2003;100:3983–8.
5. Dean M, Fojo T, Bates S. Tumour stem cells and drug resistance. Nat Rev Cancer 2005;5:275–84.
6. Bao S, Wu Q, McLendon RE, et al. Glioma stem cells promote radioresistance by preferential activation of the DNA damage response. Nature 2006;444:756–60.
7. Abraham BK, Fritz P, McClellan M, Hauptvogel P, Athelogou M, Brauch H. Prevalence of CD44+/CD24-/low cells in breast cancer may not be associated with clinical outcome but may favor distant metastasis. Clin Cancer Res 2005;11:1154–9.
8. Goodell MA, Brose K, Paradis G, Conner AS, Mulligan RC. Isolation and functional properties of murine hematopoietic stem cells that are replicating *in vivo*. J Exp Med 1996;183:1797–806.
9. Shimano K, Satake M, Okaya A, et al. Hepatic oval cells have the side population phenotype defined by expression of ATP-binding cassette transporter ABCG2/BCRP1. Am J Pathol 2003;163:3–9.
10. Falciatori I, Borsellino G, Haliassos N, et al. Identification and enrichment of spermatogonial stem cells displaying side-population phenotype in immature mouse testis. FASEB J 2004;18:376–8.
11. Asakura A, Seale P, Girgis-Gabardo A, Rudnicki MA. Myogenic specification of side population cells in skeletal muscle. J Cell Biol 2002;159:123–34.
12. Chiba T, Kika K, Zheng YW, et al. Side population purified from hepatocellular carcinoma cells harbors cancer stem cell-like properties. Hepatology 2006;44:240–51.
13. Kondo T, Setoguchi T, Taga T. Persistence of a small subpopulation of cancer stem-like cells in the C6 glioma cell line. Proc Natl Acad Sci U S A 2004;101:781–6.
14. Patrawala L, Calhoun T, Schneider-Broussard R, Zhou J, Claypool K, Tang DG. Side population is

enriched in tumorigenic, stem-like cancer cells, whereas ABCG2+ and ABCG2- cancer cells are similarly tumorigenic. Cancer Res 2005;65:6207–19.
15. Higgins CF. Multiple molecular mechanisms for multidrug resistance transporters. Nature 2007;446:749–57.
16. Chiba T, Zheng YW, Kita K, et al. Enhanced self-renewal capability in hepatic stem/progenitor cells drives cancer initiation. Gastroenterology 2007;133:937–50.
17. Iwama A, Oguro H, Negishi M, et al. Enhanced self-renewal of hematopoietic stem cells mediated by the polycomb gene product Bmi-1. Immunity 2004;21:843–51.
18. Lessard J, Sauvageau G. Polycomb group genes as epigenetic regulators of normal and leukemic hemopoiesis. Exp Hematol 2003;31:567–85.
19. Jamieson CH, Weissman IL, Passegue E. Chronic versus acute myelogenous leukemia: a question of self-renewal. Cancer Cell 2004;6:531–3.
20. Kato Y, Iwama A, Tadokoro Y, et al. Selective activation of STAT5 unveils its role in stem cell self-renewal in normal and leukemic hematopoiesis. J Exp Med 2005;202:169–79.
21. Kitamura T, Koshino Y, Shibata F, et al. Retrovirus-mediated gene transfer and expression cloning: powerful tools in functional genomics. Exp Hematol 2003;31:1007–14.
22. Oguro H, Iwama A, Morita Y, Kamijo T, van Lohuizen M, Nakauchi H. Differential impact of Ink4a and Arf on hematopoietic stem cells and their bone marrow microenvironment in Bmi1-deficient mice. J Exp Med 2006;203:2247–53.
23. Fukai K, Yokosuka O, Imazeki F, et al. Methylation status of p14ARF, p15INK4b, and p16INK4a genes in human hepatocellular carcinoma. Liver Int 2005;25:1209–16.
24. Haraguchi N, Utsunomiya T, Inoue H, et al. Characterization of a side population of cancer cells from human gastrointestinal system. Stem Cells 2006;24:506–13.
25. Ma S, Chan KW, Hu L, et al. Identification and characterization of tumorigenic liver cancer stem/progenitor cells. Gastroenterology 2007;132:5242–56.
26. Sparmann A, van Lohuizen M. Polycomb silencers control cell fate, development and cancer. Nat Rev Cancer 2006;6:846–56.
27. Valk-Lingbeek ME, Bruggeman SWM, van Lohuizen M. Stem cells and cancer: the polycomb connection. Cell 2004;118:409–18.
28. Park IK, Qian D, Kiel M, et al. Bmi-1 is required for maintenance of adult self-renewing haematopoietic stem cells. Nature 2003;423:302–5.
29. Molofsky AV, Pardal R, Iwashita T, Park IK, Clarke MF, Morrison SJ. Bmi-1 dependence distinguishes neural stem cell self-renewal from progenitor proliferation. Nature 2003;425:962–7.
30. Lessard J, Sauvageau G. Bmi-1 determines the proliferative capacity of normal and leukaemic stem cells. Nature 2003;423:255–60.
31. Liu S, Dontu G, Mantle ID, et al. Hedgehog signaling and Bmi-1 regulate self-renewal of normal and malignant human mammary stem cells. Cancer Res 2006;66:6063–71.
32. Prince ME, Sivanandan R, Kaczorowski A, et al. Identification of a subpopulation of cells with cancer stem cell properties in head and neck squamous cell carcinoma. Proc Natl Acad Sci U S A 2007;104:973–8.
33. Al-Hajj M, Clarke MF. Self-renewal and solid tumor stem cells. Oncogene 2004;23:7274–82.
34. Park IK, Morrison SJ, Clarke MF. Bmi1, stem cells, and senescence regulation. J Clin Invest 2004;113:175–9.
35. Collado M, Blasco MA, Serrano M. Cellular senescence in cancer and aging. Cell 2007;130:223–33.
36. Cagatay T, Ozturk M. P53 mutation as a source of aberrant β-catenin accumulation in cancer cells. Oncogene 2002;21:7971–80.
37. Yang ZF, Ho DW, Ng MN, et al. Significance of CD90+ cancer stem cells in human liver cancer. Cancer Cell 2008;13:153–66.

Hemodynamic Features of Gastrorenal Shunt:
A Doppler Study in Cirrhotic Patients with Gastric Fundal Varices[1]

Hitoshi Maruyama, MD, Hidehiro Okugawa, MD, Hiroaki Yoshizumi, MD, Satoshi Kobayashi, MD, Osamu Yokosuka, MD

Rationale and Objectives. Little is known about the hemodynamics of gastrorenal shunt (GRS), a major drainage route of gastric fundal varices (FV), in patients with FV. The aim of this study was to clarify the hemodynamic features of GRS on Doppler sonography in relation to the grading and bleeding of FV.

Materials and Methods. The study subjects consisted of 69 cirrhotic patients with FV. Diameter, flow velocity (FVe), and flow volume (FVo) of GRS were measured by Doppler ultrasound (US). The detection rate was compared to contrast-enhanced computed tomography (CECT), and percutaneous transhepatic portography (PTP) was used in six patients without GRS on CECT.

Results. The use of CECT detected GRS in 60 of 69 patients, and US, 58 of 69 patients. A false-negative result for detecting GRS on both CECT and US was found in one patient after PTP. The diameter, FVe, and FVo of GRS increased according to the endoscopic grade of FV: F1 (7.2 ± 1.3 mm, 9.8 ± 1.1 cm/s, 358.3 ± 123.4 ml/min), F2 (9.9 ± 3.3 mm, 12.8 ± 5.1 cm/s, 701.7 ± 411.3 ml/min), and F3 (11.8 ± 2.4 mm, 17.9 ± 8.3 cm/s, 1706.6 ± 989.5 ml/min). A significant difference was seen between F1 and F3 (diameter, $P = .0022$; FVe, $P = .0133$; FVo, $P = .0007$) and between F2 and F3 (FVe, $P = .0112$; FVo, $P < .0001$). FVe of GRS was significantly higher in bleeders (16.7 ± 8.1 cm/s) than in nonbleeders (12.2 ± 5.4 cm/s, $P = .017$), whereas the diameter and FVo were not significant.

Conclusion. Hemodynamics of GRS on Doppler sonograms reflected the grading and bleeding of FV. Doppler US may be valuable as a noninvasive method to evaluate the severity of FV.

Key Words. Gastric varices; portal hypertension; Doppler ultrasound; gastrorenal shunt.

Gastric fundal varices (FV) are known to be a considerable complication in patients with portal hypertension (1,2). Although the rates of bleeding for FV have been reported to be lower than those for esophageal varices (EV), rupture from FV sometimes results in serious consequences in the clinical course (3,4). Certain treatment methods using endoscopy, interventional techniques, and surgical procedures have been introduced for FV (5–19). However, a few studies have reported risk factors for FV bleeding, and hemodynamic features associated with FV bleeding have not been clarified (1,20,21).

There are a number of inflow vessels into FV: the left gastric, posterior gastric, and short gastric veins (22–26). The main outflow pathway in the majority of FV is the gastrorenal shunt (GRS), and the blood flow manner of GRS may represent the clinical condition of FV. Watanabe et al. (25), using the percutaneous transhepatic portography (PTP) technique, reported that the diameter of the GRS depended on the severity of FV. However, that study was based on a nonphysiologic condition using portal venous catheterization, and it lacked quantitative assessment. Little is known about

Acad Radiol 2008; 15:1148–1154

[1] From the Department of Medicine and Clinical Oncology, Chiba University Graduate School of Medicine, 1-8-1, Inohana, Chuou-ku, Chiba, 260-8670, Japan. Received December 11, 2007; accepted March 8, 2008. **Address correspondence to:** H.M. e-mail: maru-cib@umin.ac.jp

doi:10.1016/j.acra.2008.03.008

the physiologic hemodynamic features of the GRS in patients with FV.

Pulsed and color Doppler ultrasound (US) allows the real-time observation of the portal hemodynamics in patients with portal hypertension, repeatedly and noninvasively, with quantitative evaluation (27–29). The recent study demonstrated the portal systemic shunt through the renal vein on sonograms (30,31). Using this technique, we designed the present study to investigate the physiology of GRS in patients with FV. The aim of this study was to clarify the hemodynamics of GRS on Doppler sonography in relation to the grading and bleeding of FV.

MATERIALS AND METHODS

Patients

There were 76 consecutive patients with FV confirmed by endoscopic examination in our hospital between December 1999 and August 2007. Among them, seven patients received endoscopic treatment before the hemodynamic evaluation using US because of active bleeding from the FV. Therefore, 69 patients with FV formed the subject group in this retrospective study. They consisted of 36 men and 33 females, aged 41 to 80 years (mean age, 61.5 ± 8.9), and their body mass index (BMI) was 22.5 ± 4.1 kg/m^2 (range, 16.8 to 30.9). All of them had liver cirrhosis diagnosed on the basis of imaging findings, histologic findings, clinical symptoms, and biochemistry findings. The cause of liver cirrhosis was viral in 44 patients (hepatitis virus C, 40; hepatitis virus B, 4), alcohol in 9, nonalcoholic steatohepatitis (NSAH) in 3, autoimmune in 1, primary biliary cirrhosis in 3, and cryptogenic in 9. The severity of liver dysfunction, as classified according to the Child-Pugh scoring system (32), was A in 30, B in 26, and C in 13 patients. Eighteen patients had hepatocellular carcinoma (HCC), which was being controlled by nonsurgical treatment, and none had thrombus or tumor thrombus in the portal vein on US and contrast-enhanced computed tomography (CECT). Informed written consent was obtained from all patients. The preliminary step for ethics committee in our hospital deemed this retrospective study as appropriate design without approval.

Endoscopy

Endoscopic findings of FV and EV were classified according to the General Rules for Recording Endoscopic Findings set by the Japan Research Society for Portal Hypertension (33)—F1 (straight), F2 (winding), and F3 (nodule-beaded), corresponding to the grades of small, medium, and large, respectively. The grades of FV were F1 in 10, F2 in 38, and F3 in 21 patients; 24 of the FV patients were accompanied by EV, F1 in 14, and F2 in 10. All patients had primary FV, and there was no secondary FV developed after the obliteration of esophageal varices. Twenty patients were bleeders—6 were confirmed by emergency endoscopy and 14 were confirmed by clinical symptoms of hematemesis or melena. The former six bleeders received endoscopic cyanoacrylate injection therapy to attain hemostasis after the US examination. The latter 14 bleeders underwent endoscopic examination within 2 weeks after their symptoms, and another cause for gastrointestinal bleeding was not found except for FV. The remaining 49 were nonbleeders with no history of hematemesis or melena.

Contrast-enhanced Computed Tomography

CECT with dynamic study was performed in all patients using either a Somatom Plus 4 (Siemens Medical Systems, Erlangen, Germany) or a Lightspeed Ultra16 (GE Medical Systems, Milwaukee, WI) with the injection of 100 ml of contrast medium at 3 ml/s from the antecubital vein via mechanical power injector. The acquisition parameters of computed tomographic examination were 140 kV, 200 mA, scan time 0.75 s/rotation, and beam pitch 1.5 for Somatom Plus 4, and 120 kV, 350 mA (CT-AEC), scan time 0.8 s/rotation, beam pitch 1.375, and collimation 0.625 mm for Lightspeed Ultra16. Scanning was performed with a 30-s delay between contrast administration and start of scanning for the hepatic artery−dominant phase, 80-s delay for the portal vein−dominant phase, and 180-s delay for the equilibrium phase. The computed tomographic image was evaluated by one of the authors (H.O.).

Ultrasound

Equipment and settings.—The US systems used in the present study were SSA-380A, 390A, and 770A (Toshiba, Tokyo, Japan), which were the high-end systems during the study period, with a 3.75-MHz convex probe. The imaging modes were gray-scale B-mode US, pulsed Doppler US, and color flow imaging. Pulsed Doppler US was used for the measurement of mean flow velocity (FVe, centimeters per second) and mean flow volume (FVo, milliliters per minute), with sampling width corresponding to the maximum diameter of the vessel and at an angle less than 60° between the US beam

and the vessel. Color flow imaging was done with an optimal level of gain and at 65 dB of dynamic range, and these settings were used in all examinations. US examination was performed in the spine position and a fasting state of over 6 hours (except for the bleeders) and patients were asked to breathe normally.

Demonstration of gastrorenal shunt.—At first, the left renal vein was detected with a long-axis view on the sonogram by transverse scan in the middle part of the abdomen. Then, the probe was turned clockwise approximately 90° for a sagittal scan at the left side of the abdominal aorta. The GRS on the sonogram was defined as the vessel that communicated with the left renal vein running beside the abdominal aorta with a long-axis view. When the GRS was not observed on the image, the probe was tilted gently from side to side. After the presence and direction of blood flow were confirmed by color flow imaging, the maximum diameter of GRS was measured on the gray-scale sonogram and blood flow was measured by pulsed Doppler US. The sensitivity and specificity of US in detecting GRS for CT were evaluated. All US examinations were performed by one of the authors (H.M., a specialist in gastroenterology and hepatology with a 14-year career with Doppler US), and all digitally stored sonograms on the magneto-optical disk were reviewed at a later date by two of the authors (S.K. and H.Y.). A second US examination within 1 week (4 to 7 days) after the initial one was done in 13 patients who had sufficient time before prophylactic treatment, and intraobserver variability for the measurement results of GRS was calculated. US examinations were performed before the treatment for FV in all patients.

Percutaneous Transhepatic Portography

Portal vein catheterization was performed by means of a US-guided procedure (34), and a portogram was obtained during the injection of contrast medium into the splenic hilum.

Statistical Analysis

All results were expressed as mean ± standard deviation or percentage. All statistical analysis was performed using the StatView for Windows (version 5.0J; SAS Institute Inc., Cary, NC). Fisher's protected least-significant difference (PLSD) was used to compare the diameter, FVe, and FVo of GRS with the grade of FV, Child's classification, or causes of liver cirrhosis, and the Mann-Whitney *U*-test was used to compare the diameter, FVe, and FVo of GRS with the presence of EV or bleeding of FV. Significance was taken at $P < .05$ for all tests.

RESULTS

Comparison of the Detection Rate of Gastrorenal Shunt Between Ultrasound and Contrast-enhanced Computed Tomography

On US, the sagittal plane demonstrated a long-axis view of the GRS from the cranial and dorsal side to the caudal and ventral side, which connects into the left renal vein (Fig. 1). GRS was detected by US in 58 patients (58 of 69, 84.1%) and by CECT in 60 patients (60 of 69, 87%). US failed to detect GRS in two CECT-positive patients, likely because of excessive gas in the gastrointestinal tract. The sensitivity and specificity of US in detecting CECT detected GRS were 96.7% and 100%, respectively.

Forty-two patients required curative treatment for FV—20 with a bleeding history and 22 who hoped for prophylaxis for middle-sized or large FV. Drainage route of FV was clearly demonstrated on CECT and/or US in 36 patients—the GRS in 35 and inferior phrenic vein (IPV) in one. The other 6 patients for whom the drainage route was not demonstrated on the images underwent PTP for pretreatment portal hemodynamics evaluation. The portogram revealed the presence of GRS with a partially narrowed appearance in one patient (see Fig. 2), and the remaining five patients had other vessels for the drainage route of FV—the azygos vein in three and the IPV in two. Therefore, 39 patients underwent balloon-occluded retrograde transvenous obliteration (B-RTO) from the drainage routes of FV (GRS in 36 patients and IPV in 3 patients), and the other 3 patients were followed up without additional treatment.

Hemodynamic Features of Gastrorenal Shunt on the Sonograms

GRS on the sonograms showed flow direction continuously toward the left renal vein in 53 patients, but a to-and-fro appearance was observed in the other five patients (F1 in 2 and F2 in 3; Fig. 3).

The diameter, FVe, and FVo of GRS increased according to the endoscopic grade of FV in 53 patients without a to-and-fro appearance (Table 1): F1 (7.2 ± 1.3 mm, 9.8 ± 1.1 cm/s, 358.3 ± 123.4 ml/min), F2 (9.9 ± 3.3 mm, 12.8 ± 5.1 cm/s, 701.7 ± 411.3 ml/min), and F3 (11.8 ± 2.4 mm, 17.9 ± 8.3 cm/s, 1706.6 ± 989.5 ml/min). A

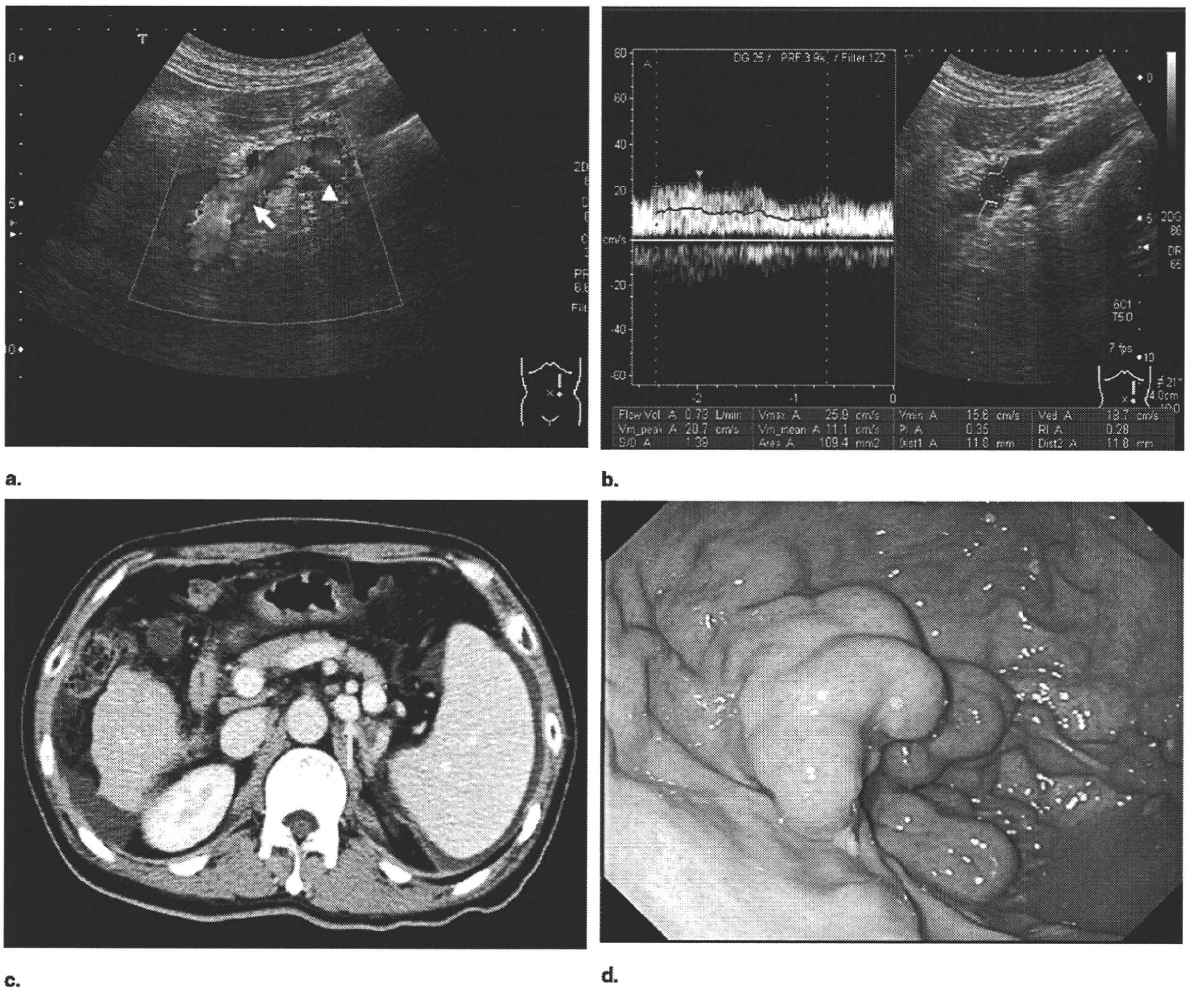

Figure 1. Demonstration of gastrorenal shunt (GRS) on Doppler ultrasound and contrast-enhanced computed tomography (CECT) images in patient with gastric fundal varices (52-year-old man). **(a)** The sagittal plane of the color Doppler sonogram demonstrated a long-axis view of GRS (*arrow*) from the cranial and dorsal side to the caudal and ventral side, which connects into the left renal vein (*arrowhead*) with a flow direction continuously toward the left renal vein. **(b)** Pulsed Doppler. Flow velocity and flow volume were measured by the pulsed Doppler method. **(c)** CECT. CECT demonstrated GRS at the left side of the abdominal aorta (*arrow*). **(d)** Endoscopy. This patient had large-grade FV (F3).

significant difference was seen between F1 and F3 (diameter, $P = .0022$; FVe, $P = .0133$; FVo, $P = .0007$; Fisher's PLSD) and between F2 and F3 (FVe, $P = .0112$; FVo, $P < .0001$; Fisher's PLSD). However, the diameter, FVe, and FVo showed no significant difference between patients with EV and patients without EV, and in relation to the causes of liver cirrhosis. FVe of GRS was significantly higher in bleeders (16.7 ± 8.1 cm/s) than in nonbleeders (12.2 ± 5.4 cm/s, $P = .017$, Mann-Whitney *U*-test; Table 2), whereas the diameter and FVo were not significant. The diameter, FVe, and FVo of GRS also increased according to the progression of Child's classification: A (9.0 ± 2.4 mm, 12.2 ± 5.5 cm/s, 819.9 ± 521.6 ml/min), B (10.3 ± 3.3 mm, 13.6 ± 4.9 cm/s, 791.3 ± 578.4 ml/min), and C (11.9 ± 2.8 mm, 19.7 ± 9.9 cm/s, 1610 ± 996.7 ml/min). FVe between Child A and C ($P = .015$, Fisher's PLSD) and FVo between Child A and C ($P = .023$, Fisher's PLSD) and between B and C ($P = .035$, Fisher's PLSD) were significantly different. Intraobserver variability for the measurement results of GRS was 5.2% for diameter, 7.7% for FVe, and 9.3% for FVo.

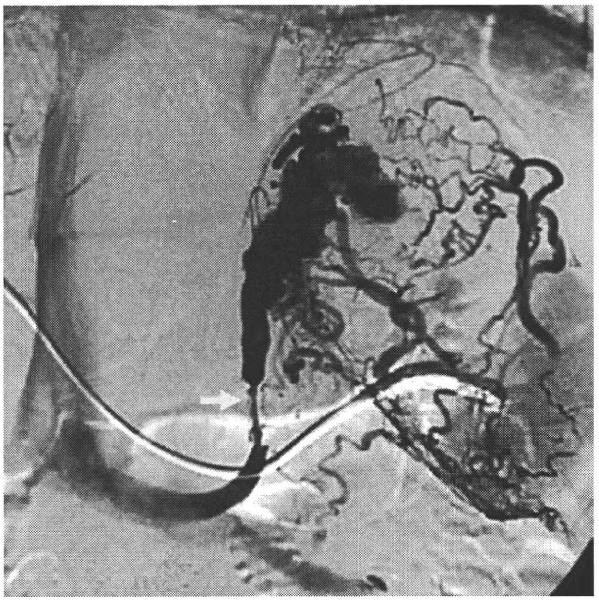

Figure 2. A portogram showing a gastrorenal shunt (GRS) with a linear stricture (*arrow*). Neither ultrasound nor contrast-enhanced computed tomography demonstrated GRS in this case.

DISCUSSION

The present study is probably the first to report on the physiologic hemodynamics of GRS, a main outflow route of FV, in relation to the condition of FV. Gray-scale US detected GRS using a longitudinal scan with a long-axis view at the left side of the abdominal aorta, and Doppler US dramatically demonstrated real-time blood flow imaging. Quantitative assessment of the hemodynamics of GRS was successfully conducted by this method in cirrhotic patients with FV.

As for the detection rate of GRS, US showed a similar rate to that of CECT for the visualization of GRS. Although there is little doubt that three-dimensional computed tomographic images can be useful for the detection of GRS (22), excessive exposure to x-rays has become a major problem worldwide. Application of CECT only for the purpose of detecting GRS in patients with FV may be limited to those in whom GRS is not detected by US. However, as visualization on the sonograms depends on the physical size of the patients, the detectability of GRS may vary by race. Contrast-enhanced US with microbubble contrast agents might be a worthwhile option for improving the detectability of the blood flow of GRS (29).

We had nine cases whose GRS was not demonstrated on CECT and US images. Portal venous hemodynamics was examined by PTP in six of them, and the GRS in one case had a partial linear stricture that was considered to be the reason for the detection failure on US and CECT. Although such a case might be rare in clinical practice, advancement of the balloon catheter without this information beforehand would be a dangerous maneuver during B-RTO. If US/CT does not show the existence of GRS, PTP or arterial portography should be performed for the confirmation of the presence and patency of GRS. GRS might be present in our three other cases without GRS according to CECT and US. In addition, our method may need to be compared with magnetic resonance imaging, which is also useful for the evaluation of portal hemodynamics.

B-RTO has received considerable attention recently as an effective method for the treatment of FV (8−10). Because the application of this technique depends on the presence of GRS, our method may prove useful for deciding the therapeutic strategy in patients with FV. In addition, measurement of the diameter of GRS might help in balloon size selection for the GRS occlusion during B-RTO. The IPV is also a drainage route to which B-RTO can be applied in patients with FV, although it is less common than GRS (9,10). The present study had three cases with IPV, and only one of them was visible by US. Although there may be an anatomic reason for missing these, the poor visualization of IPV on a sonogram is a shortcoming of our method.

Flow velocity and flow volume of GRS corresponded to the endoscopic grade of FV and liver function, and these results may suggest that the hemodynamics of GRS depend on the development of hepatofugal collateral blood flow. However, there was no significant difference in the parameters of GRS between small-grade FV (F1) and medium-grade FV (F2). This might be explained by the exponential hemodynamic change between F2 and F3 in the progressing course of FV from F1 to F3. However, as a small number of patients with F1 grade might affect this statistical result, further study would be necessary to clarify this point.

Meanwhile, the measured parameters of GRS by Doppler US did not show any significant difference between patients with EV and patients without EV, and in relation to the causes of cirrhosis. The hemodynamics of GRS might be specific to the FV itself, regardless of the presence of the EV and the causes of cirrhosis.

Our study had five cases with GRS in which the blood flow direction appeared as to-and-fro on color Doppler imaging. This physiologic phenomenon has not been doc-

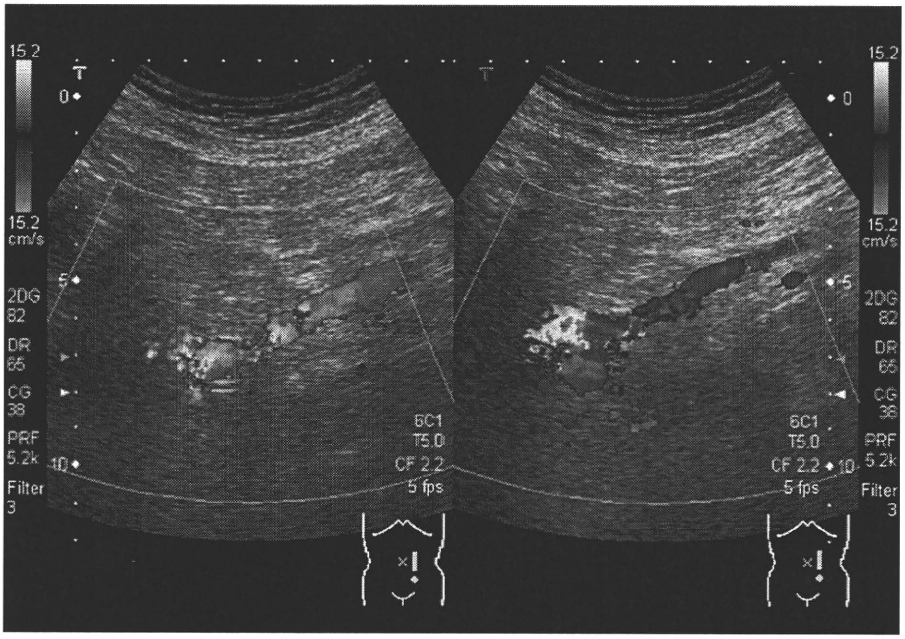

Figure 3. Color Doppler (72-year-old man with medium-grade gastric fundal varices [F2]). The sagittal plane of the color Doppler sonogram showed gastrorenal shunt with a to-and-fro appearance.

Table 1
Hemodynamics in the Gastrorenal Shunt (GRS) in Relation to the Grade of Gastric Fundal Varices

	GRS (mean ± SD)		
FV	Diameter (mm)	FVe (cm/s)	FVo (mL/m)
F1	7.2 ± 1.3*	9.8 ± 1.1‡	358.3 ± 123.4**
F2	9.9 ± 3.3†	12.8 ± 5.1§	701.7 ± 411.3††
F3	11.8 ± 2.4*†	17.9 ± 8.3‡§	1706.6 ± 989.5**††

FVe: flow velocity; FVo: flow volume.
*P = .0022; †P = .0515; ‡P = .0133; §P = .0112; **P = .0007; ††P < .0001 (Fisher's PLSD).

Table 2
Hemodynamics in the Gastrorenal Shunt (GRS) in Relation to the Bleeding of Gastric Fundal Varices

	GRS (mean ± SD)		
	Diameter (mm)	FVe (cm/s)	FVo (mL/m)
Nonbleeder	10.2 ± 3.5*	12.2 ± 5.4†	843.8 ± 810.3‡
Bleeder	10.3 ± 2.5*	16.7 ± 8.1†	1187.1 ± 914.2‡

FVe: flow velocity; FVo: flow volume.
*‡Nonsignificant; †P = .017 (Mann-Whitney U-test).

umented elsewhere, and it may not be demonstrated except by Doppler US examination. The authors speculate that low portal venous pressure and/or additional hemodynamic factors such as the presence of IPV might be connected with this phenomenon, although the cause for this hemodynamic remains to be unraveled.

High PVP is not always a risk factor for FV bleeding (13,16), and it has been reported that PVP decreased according to the development of GRS (25). These characteristic features in the FV may support the findings that the diameter and FVo of GRS did not show significant difference between bleeders and nonbleeders in the present study. However, our results have shown that the flow velocity of GRS in bleeders was significantly higher than that in nonbleeders. Doppler US might be a novel option for predicting FV bleeding in the clinical course of portal hypertension.

There are some limitations to the present study. First, this is a retrospective study about the hemodynamics of GRS at one time in patients with FV. Changes in the hemodynamics of GRS during the long-term clinical course and their correlation with the endoscopic findings, bleeding of FV, and changes of liver function are aspects of great interest in this field. Second, a single operator performed the US examinations in the present study. Although a constant technique for blood flow measurement

may provide highly reliable results and sufficient intraobserver variability was obtained, interobserver variability would also be an important factor for evaluating the methodology. This needs to be examined in further studies. Third, shunt to the renal vein accounts for the drainage pathway in some portosystemic collateral vessels without forming FV in patients with portal hypertension (26,30,31,35). The clinical value of US examination in these patients should be clarified.

CONCLUSION

Our study clarified that the hemodynamic features of GRS under physiologic conditions using Doppler US in cirrhotic patients with FV. Although a prospective study with a large number of patients is needed, this simple and noninvasive technique might be valuable for the clinical management of FV, assessment of its severity, and bleeding risk.

REFERENCES

1. Sarin SK, Lahoti D, Saxena SP, et al. Prevalence, classification and natural history of gastric varices: A long-term follow-up study in 568 portal hypertension patients. Hepatology 1992; 16:1343–1349.
2. Bosch J, Abraldes JG, Groszmann R. Current management of portal hypertension. J Hepatol 2003; 38:S54–S68.
3. Ryan BM, Stockbrugger RW, Ryan JM. A pathophysiologic, gastroenterologic, and radiologic approach to the management of gastric varices. Gastroenterology 2004; 126:1175–1189.
4. Lubel JS, Angus PW. Modern management of portal hypertension. Intern Med J 2005; 35:45–49.
5. D'amico G, Pagliaro L, Bosch J. The treatment of portal hypertension: A meta-analytic review. Hepatology 1995; 22:332–354.
6. Greenwald BD, Caldwell SH, Hespenheide EE, et al. *N*-2-Butyl-cyanoacrylate for bleeding gastric varices: A United States pilot study and cost analysis. Am J Gastroenterol 2003; 98:1982–1988.
7. Tripathi D, Ferguson JW, Therapondos G, et al. Review article: Recent advances in the management of bleeding gastric varices. Aliment Pharmacol Ther 2006; 24:1–17.
8. Kanagawa H, Mima S, Kouyama H, et al. Treatment of gastric fundal varices by balloon-occluded retrograde transvenous obliteration. J Gastroenterol Hepatol 1996; 11:51–58.
9. Koito K, Namieno T, Nagakawa T, et al. Balloon-occluded retrograde transvenous obliteration for gastric varices with gastrorenal or gastrocaval collaterals. AJR Am J Roentgenol 1996; 167:1317–1320.
10. Akahane T, Iwasaki T, Kobayashi N, et al. Changes in liver function parameters after occlusion of gastrorenal shunts with balloon-occluded retrograde transvenous obliteration. Am J Gastroenterol 1997; 92:1026–1030.
11. Yamagami T, Kato T, Iida S, et al. Change in the hemodynamics of the portal venous system after retrograde transvenous balloon occlusion of a gastrorenal shunt. AJR Am J Roentgenol 2003; 181:1011–1015.
12. Scott J, Dick R, Long RG, et al. Percutaneous transhepatic obliteration of gastro-oesophageal varices. Lancet 1976; 2:53–55.
13. Sanyal AJ, Freedman AM, Luketic VA, et al. The natural history of portal hypertension after transjugular intrahepatic portosystemic shunts. Gastroenterology 1997; 112:889–898.
14. Chau T, Patch D, Chan Y, et al. "Salvage" transjugular intrahepatic portosystemic shunts: Gastric fundal compared with oesophageal variceal bleeding. Gastroenterology 1998; 114:981–987.
15. Barange K, Peron JM, Imani K, et al. Transjugular intrahepatic portosystemic shunt in the treatment of refractory bleeding from ruptured gastric varices. Hepatology 1999; 30:1139–1143.
16. Tripathi D, Therapondos G, Jackson E, et al. The role of the transjugular intrahepatic portosystemic stent shunt (TIPSS) in the management of bleeding gastric varices: Clinical and haemodynamic correlations. Gut 2002; 51:270–274.
17. Boyer T. Transjugular intrahepatic portosystemic shunt: Current status. Gastroenterology 2003; 124:1700–1710.
18. Thomas PG, D'Cruz AJ. Distal splenorenal shunting for bleeding gastric varices. Br J Surg 1994; 81:241–244.
19. Yamamoto J, Nagai M, Smith B, et al. Hand-assisted laparoscopic splenectomy and devascularization of the upper stomach in the management of gastric varices. World J Surg 2006; 30:1–6.
20. Kim T, Shijo H, Kokawa H, et al. Risk factors for hemorrhage from gastric fundal varices. Hepatology 1997; 25:307–312.
21. Akiyoshi N, Shijo H, Iida T, et al. The natural history and prognostic factors in patients with cirrhosis and gastric fundic varices without prior bleeding. Hepatol Res 2000; 17:145–155.
22. Matsumoto A, Kitamoto M, Imamura M, et al. Three-dimensional portography using multislice helical CT is clinically useful for management of gastric fundic varices. AJR Am J Roentgenol 2001; 176:899–905.
23. Ono N, Toyonaga A, Nishimura H, et al. Evaluation of magnetic resonance angiography on portosystemic collaterals in cirrhotic patients. Am J Gastroenterol 1997; 92:1515–1519.
24. Anderson CM. GI magnetic resonance angiography. Gastrointest Endosc 2002; 55:S42–S48.
25. Watanabe K, Kimura K, Matsutani S, et al. Portal hemodynamics in patients with gastric varices: A study in 230 patients with esophageal and/or gastric varices using portal vein catheterization. Gastroenterology 1988; 95:434–440.
26. Kimura K, Ohto M, Matsutani S, et al. Relative frequencies of portosystemic pathways and renal shunt formation through the "posterior" gastric vein: Portographic study in 460 patients. Hepatology 1990; 12:725–728.
27. Grant EG, Tessler FN, Perrella RR. Clinical Doppler Imaging. AJR Am J Roentgenol 1989; 152:707–717.
28. Schmassmann A, Zuber M, Livers M, et al. Recurrent bleeding after variceal hemorrhage: Predictive value of portal venous duplex sonography. AJR Am J Roentgenol 1993; 160:41–47.
29. Ferrara K, Deangelis G. Color flow mapping. Ultrasound Med Biol 1997; 23:321–345.
30. von Herbay A, Frieling T, Haeussinger D. Color Doppler sonographic evaluation of spontaneous portosystemic shunts and inversion of portal venous flow in patients with cirrhosis. J Clin Ultrasound 2000; 28:332–339.
31. Yamada M, Ishida H, Komatsuda T, et al. Portal systemic shunt through the renal vein. Abdom Imaging 2006; 31:701–705.
32. Pugh RN, Murray-Lyon IM, Dawson JL, et al. Transection of the esophagus for bleeding esophageal varices. Br J Surg 1973; 60:646–649.
33. The Japan Society for Portal Hypertension. The General Rules for Study of Portal Hypertension, ed 2. Tokyo, Japan: Kanehara & Co., Ltd. 2004:37–50.
34. Kimura K, Tsuchiya Y, Ohto M, et al. Single-puncture method for percutaneous transhepatic portography using a thin needle. Radiology 1981; 139:748–749.
35. Takayasu K, Moriyama N, Shima Y, et al. Sonographic detection of large spontaneous spleno-renal shunts and its clinical significance. Br J Radiol 1984; 57:565–570.